

AIR: Zero-shot Generative Model Adaptation with Iterative Refinement

Guimeng Liu Milad Abdollahzadeh Ngai-Man Cheung*
 Singapore University of Technology and Design (SUTD)
 {guimeng_liu,milad_abdollahzadeh,ngaiman_cheung}@sutd.edu.sg

Abstract

*Zero-shot generative model adaptation (ZSGM) aims to adapt a pre-trained generator to a target domain using only text guidance and without any samples from the target domain. Central to recent ZSGM approaches are directional loss which use the text guidance in the form of aligning the image offset with text offset in the embedding space of a vision-language model like CLIP. This is similar to the analogical reasoning in NLP where the offset between one pair of words is used to identify a missing element in another pair by aligning the offset between these two pairs. However, a major limitation of existing ZSGM methods is that the learning objective assumes the complete alignment between image offset and text offset in the CLIP embedding space, resulting in quality degrade in generated images. **Our work** makes two main contributions. Inspired by the offset misalignment studies in NLP, as our first contribution, we perform an empirical study to analyze the misalignment between text offset and image offset in CLIP embedding space for various large publicly available datasets. Our important finding is that offset misalignment in CLIP embedding space is correlated with concept distance, i.e., close concepts have a less offset misalignment. To address the limitations of the current approaches, as our second contribution, we propose Adaptation with Iterative Refinement (AIR) which is the first ZSGM approach to focus on improving target domain image quality based on our new insight on offset misalignment. **Qualitative, quantitative, and user study in 26 experiment setups consistently demonstrate the proposed AIR approach achieves SOTA performance. Additional experiments are in Supp. Our code is released here: <https://github.com/Guimeng-Leo-Liu/AIR>.***

1. Introduction

Generative models like Generative Adversarial Networks (GANs) [3, 18, 22, 24] and Diffusion Models [10, 42, 49]

have recently shown promising results in image generation with significant advancements in the fidelity and diversity of the generated images. Training these generative models typically requires large amounts of data (e.g., 70K images required for training StyleGAN2 [25] or 400M images used for training Latent Diffusion Model [49]). However, in many real-world scenarios, a limited amount of data is available from the target domain (e.g., medical domains, rare animal species, and artistic domains). Training a generative model under this limited data regime is extremely challenging, resulting in issues like mode collapse or quality degradation [1]. To address this, *generative model adaptation* is an active research area to adapt a pre-trained generator to a new target domain with limited data [32, 35, 36, 43, 55, 60–62, 65–67]. Taking this one step further, a recent task *zero-shot generative model adaptation* (ZSGM) [15, 19, 21] shifts a pre-trained model to a target domain using only text guidance (no target domain image).

ZSGM with Offset Alignment. NADA [15] is the pioneering work that uses text offset between source and target domains in CLIP embedding space as guidance to shift a pre-trained generative model to the target domain. Specifically, the learning objective is to align the image offset between the pre-trained generator and the adapted generator with the text offset. IPL [19] improves on this by using prompt learning to enhance diversity, addressing NADA’s limitations in image-specific feature representation. SVL [21] advances further by modeling semantic variations to tackle mode collapse and improve diversity. The idea of offset alignment has some similarities to analogical reasoning in NLP literature [33, 39–41] where the offset between one pair of word vectors is used to identify the unknown member of a different pair of words, commonly via alignment of offsets. For example the offset $E_v(\text{“Man”}) - E_v(\text{“Woman”})$ and $E_v(\text{“King”})$ being used to identify $E_v(\text{“Queen”})$, with E_v denoting vector representation in some embedding space. See Supp. Sec. L for detailed discussion on related work.

Research Gap. All current ZSGM approaches [15, 19, 21] assume that *the image and text offsets are completely aligned in the CLIP embedding space* and leverage this in

*Corresponding author

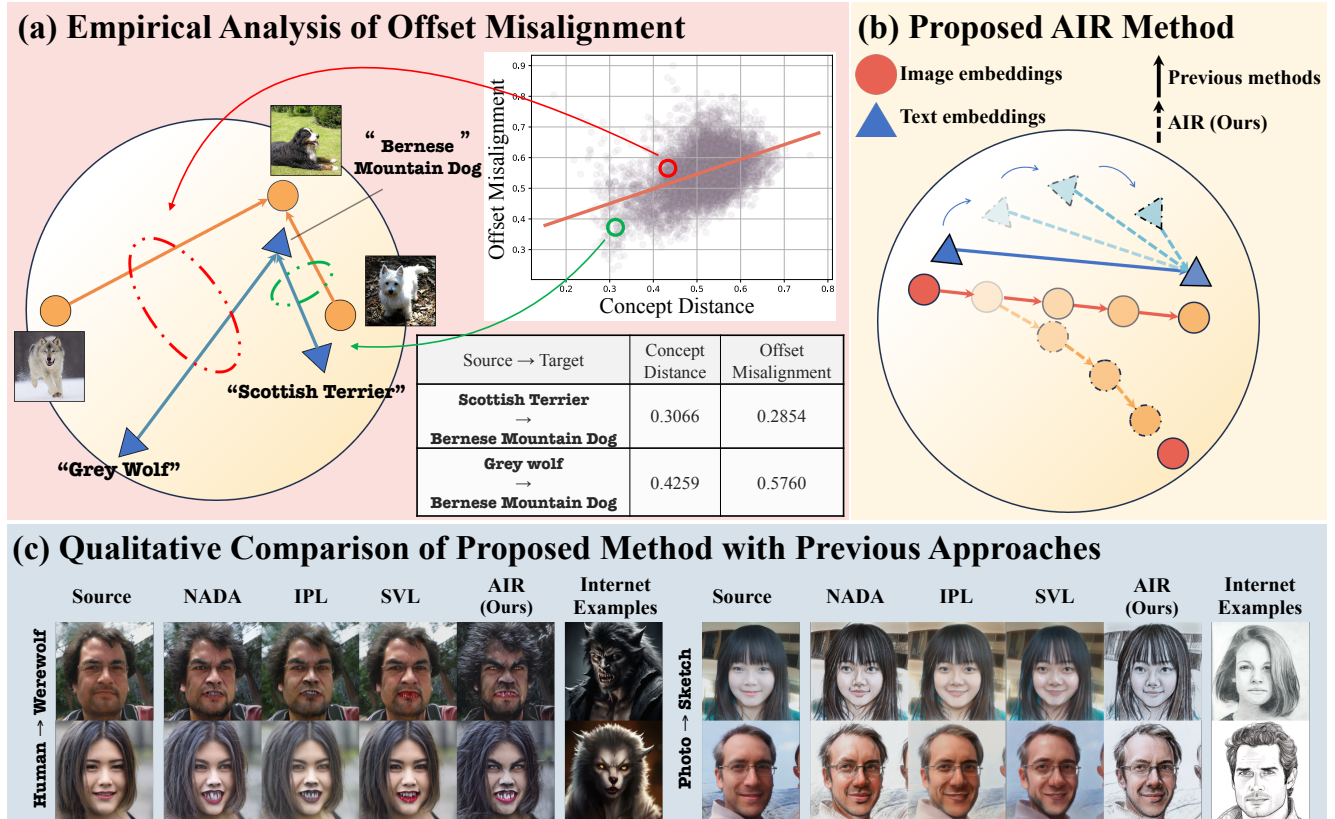


Figure 1. **Our contributions:** (a) For the first time in the literature, we perform a comprehensive analysis of offset misalignment in CLIP embedding space. Our analysis reveals that there is a misalignment between image offset (orange arrow) and text offset (blue arrow) in CLIP space. **Importantly, we discover that offset misalignment is correlated with concept distance.** For example, in the ImageNet-1K dataset, the “Grey Wolf” is a more distant concept to the “Bernese Mountain Dog” (concept distance=0.4259) than the “Scottish Terrier” (concept distance=0.3066). Accordingly, “Grey Wolf” → “Bernese Mountain Dog” has higher offset misalignment than “Scottish Terrier” → “Bernese Mountain Dog” (0.5760 vs 0.2854). This misalignment is overlooked in existing approaches, resulting in degradation in target domain image quality (see Sec. 3). (b) We propose Adaptation with Iterative Refinement (AIR) to mitigate the issue with offset misalignment. We iteratively sample anchor points closer to the target domain and use these anchors to refine the adaptation direction (Sec. 4). (c) Our proposed AIR consistently achieves SOTA performance across various adaptation setups by better capturing the target domain’s style and details. In contrast, all other methods suffer from inadequate adaptation and fail to capture rich target domain features due to offset misalignment and inaccurate guidance during generator adaptation (see Sec. 5 for detailed results).

their learning objective while adapting pre-trained generator to target domain. However, this assumption can have two major limitations: i) CLIP embedding space is trained to maximize the similarity between corresponding image-text pairs, and the degree of alignment between image and text offsets has not been studied, and ii) this degree of alignment could also vary based on the distance between source and target domains. Recalling the similarity between ZSGM with offset alignment and analogical reasoning, previous studies in NLP have shown that the accuracy of analogical reasoning increases if the concepts are nearby and similar (e.g., $E_v(\text{“King”}) E_v(\text{“Queen”})$ [14, 28, 34, 48]), and decreases when the concepts are distant.

Contributions. This paper takes an important step toward addressing the research gaps in ZSGM. *First*, we take

a closer look to analyze the offset misalignment in CLIP embedding space. Specifically, we perform an empirical study on large public datasets to analyze the degree of the offset alignment between image and text offsets in CLIP embedding space vs concept distance. **Our results suggest that offset misalignment exists in the CLIP embedding space and it increases as the concepts are more distant** (Fig. 1, (a)). Additionally, we perform a set of experiments to show that for closer source and target domains, the offset misalignment is less problematic during ZSGM. *Second*, informed by our analysis, we propose Adaptation with Iterative Refinement (AIR) to mitigate the offset misalignment issue. After limited iterations of the adaptation, the adapted generator is already closer to the target domain than the pre-trained generator (see Supp. Sec. G), and therefore

it suffers less from offset misalignment. Then, we iteratively sample anchor points during adaptation and use these anchor points to refine the offsets (Fig. 1, (b)). Since the textual description of these anchor points is unknown, we propose a new prompt learning strategy to learn these descriptions. Our main contributions are:

- We conduct a comprehensive analysis of the offset misalignment between image and text modalities in the CLIP embedding space. Our analysis reveals, for the first time in literature, a meaningful correlation between offset misalignment and concept distance.
- We propose the Adaptation with Iterative Refinement to address the offset misalignment in CLIP embedding space. Our approach includes an iterative sampling of anchor points during adaptation coupled with a new prompt learning approach to learn the textual description of these anchor points.
- Extensive experimental results show that our proposed AIR approach consistently outperforms existing ZSGM approaches achieving new SOTA performance. We remark that for the first time in the literature, we perform zero-shot adaptation for the diffusion models.

2. Preliminaries: Directional CLIP Loss

In zero-shot generative model adaptation setup [15], given a pre-trained generator G_S on the source domain \mathcal{S} , and textual descriptions of source and target domains, denoted by T_S and T_T respectively, the goal is to shift G_S to target domain \mathcal{T} to generate diverse and high-quality images from this domain [1]. For this adaptation, current approaches [15, 19, 21] use the CLIP model [47] as the source of supervision, and assume that text and image offsets (between \mathcal{S} and \mathcal{T}) are well-aligned in CLIP representation space. Therefore, the text offset is computed based on the provided textual descriptions of the source and target. Then, the trainable generator is initialized with the parameters of the G_S , and optimized in a way to align image offset with text offset, leading to the directional CLIP loss:

$$\begin{aligned} \mathcal{L}_{direction} &= 1 - \cos(\Delta I_{S \rightarrow t}, \Delta T_{S \rightarrow T}), \\ \text{where } \Delta I_{S \rightarrow t} &= E_I(G_t(w)) - E_I(G_S(w)), \\ \text{and } \Delta T_{S \rightarrow T} &= E_T(T_T) - E_T(T_S) \end{aligned} \quad (1)$$

where $\cos(x, y) = x \cdot y / |x| |y|$ represents the cosine similarity. E_T and E_I denote the CLIP text and image encoders, respectively. G_t denotes the trainable generator in iteration t of adaptation. $\Delta I_{S \rightarrow t}$ denotes the image offset computed from the source generator to the trainable generator, and $\Delta T_{S \rightarrow T}$ denotes the text offset from source to target.

3. A Closer Look at Offset Misalignment in CLIP Space

Previous works assume that for two different concepts α and β , the image offset $\Delta I_{\alpha \rightarrow \beta}$ and text offset $\Delta T_{\alpha \rightarrow \beta}$ are completely aligned in the multimodal CLIP embedding space. This assumption of perfect alignment is the foundation of the directional loss in Eq. 1. We postulate that this assumption may have two major limitations:

- CLIP [47] is trained using a contrastive loss to maximize the cosine similarity between corresponding image-text pairs, *i.e.*, maximize $\cos(E_I(I_\alpha), E_T(T_\alpha))$ for concept α (*e.g.*, cat), or maximize $\cos(E_I(I_\beta), E_T(T_\beta))$ for concept β (*e.g.*, dog). Note that the degree of alignment of image offset $\Delta I_{\alpha \rightarrow \beta}$ and text offset $\Delta T_{\alpha \rightarrow \beta}$ in CLIP space is not studied in the literature.
- In addition, this degree of alignment between $\Delta I_{\alpha \rightarrow \beta}$ and $\Delta T_{\alpha \rightarrow \beta}$ may vary based on the distance between two concepts α and β .

In this section, we take a closer look at this degree of offset alignment between two different modalities in CLIP space. First, inspired by offset misalignment in NLP, we conduct an empirical study on large public datasets to analyze the offset misalignment between image and text modalities in CLIP embedding space. Our analysis suggests that **there is a misalignment between $\Delta I_{\alpha \rightarrow \beta}$ and $\Delta T_{\alpha \rightarrow \beta}$ in CLIP embedding space, and this misalignment increases as concepts α and β become more distant**. Second, we take a further step and design an experiment to evaluate the effect of this offset misalignment in generative model adaptation using directional loss (Eq. 1). Our experimental results suggest that **less offset misalignment in CLIP embedding space leads to a better generative model adaptation with directional loss**.

3.1. Empirical Analysis of Offset Misalignment

In this section, we conduct an empirical experiment on public datasets to evaluate the degree of alignment between image and text offsets. We randomly sample two classes for each dataset as a pair of concept (α, β) . Then, the images within each class are used alongside the related textual description (*e.g.*, label) of each class to measure offset misalignment $\mathcal{M}(\alpha, \beta)$ in a similar way to directional loss:

$$\begin{aligned} \mathcal{M}(\alpha, \beta) &= 1 - \cos(\Delta I_{\alpha \rightarrow \beta}, \Delta T_{\alpha \rightarrow \beta}), \\ \text{where } \Delta I_{\alpha \rightarrow \beta} &= E_I(\overline{I_\beta}) - E_I(\overline{I_\alpha}), \\ \text{and } \Delta T_{\alpha \rightarrow \beta} &= E_T(T_\beta) - E_T(T_\alpha) \end{aligned} \quad (2)$$

where $E_I(\overline{I_\alpha})$ is the average embedding of all images of the class (concept) α in CLIP space. In addition, to measure

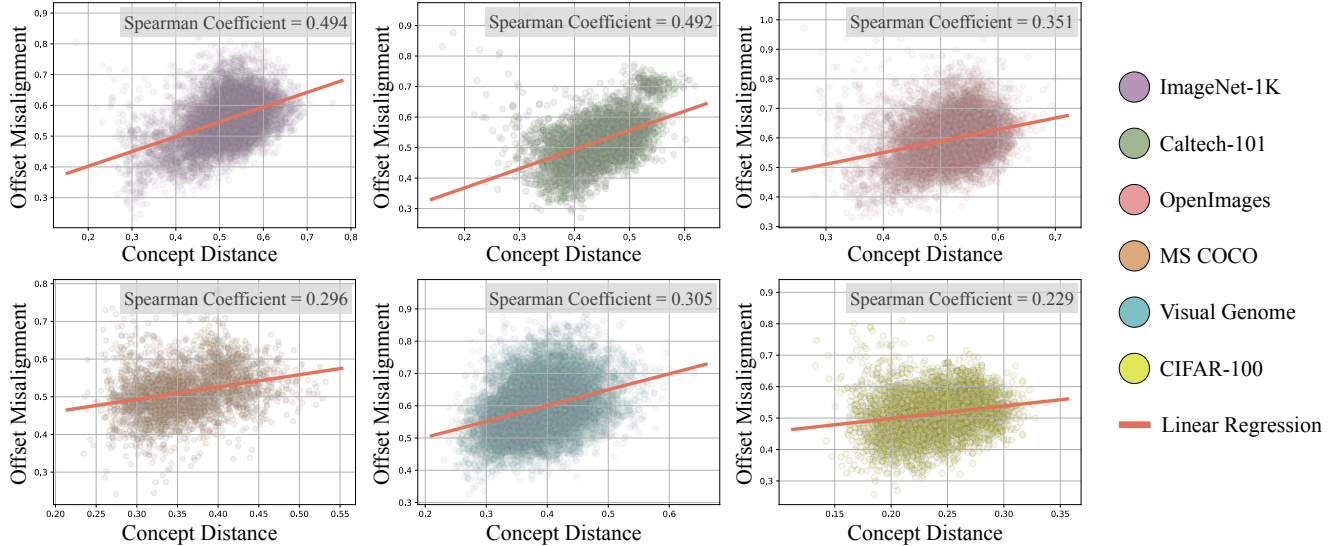


Figure 2. **Empirical analysis of offset misalignment in ViT-based CLIP space:** We plot the offset misalignment (Eq. 2) vs concept distance for $N = 5000$ of text-image pairs in CLIP space which are sampled from 6 large publicly available datasets (details in Supp. Sec. C.1). Our results show that there is a meaningful correlation (measured by Spearman’s coefficient [57]) between offset misalignment and concept distance for datasets with different distributions, i.e., close concepts has less offset misalignment. Additionally, we have analysis for CNN-based CLIP space in Supp. Sec. F.

the distance between two concepts denoted by $\mathcal{D}(\alpha, \beta)$, we use the cosine similarity between images of two classes, i.e., $\mathcal{D}(\alpha, \beta) = 1 - \cos(E_I(I_\beta), E_I(I_\alpha))$. We repeat this process to have $N = 5000$ pairs of concepts for each dataset. Then, we plot $\mathcal{M}(\alpha, \beta)$ against $\mathcal{D}(\alpha, \beta)$ for each pair of concepts.

Experimental Setup. In this experiment, we use CLIP ViT-Base/32 as the vision encoder. We use 6 large and multi-class datasets that are publicly available, including ImageNet [9], Caltech-101 [13], OpenImages [31], MS COCO [37], Visual Genome [29], and CIFAR-100 [30] (details in Supp Sec. C.1).

Results. Fig. 2 shows the offset misalignment against the concept distance for $N = 5000$ pairs of concepts for 6 public datasets. As shown in the plots, for all datasets, apart from their different distributions and characteristics, there is a correlation between offset misalignment and concept distance. Particularly, if two concepts α and β are distant, there is a higher misalignment between image offset $\Delta I_{\alpha \rightarrow \beta}$ and corresponding text offset $\Delta T_{\alpha \rightarrow \beta}$. This means that given I_α, T_α and T_β , it is sub-optimal to align $\Delta I_{\alpha \rightarrow \beta}$ and $\Delta T_{\alpha \rightarrow \beta}$ to find I_β . On the other hand, if two concepts α and β are closer, potentially, it is more accurate to align $\Delta I_{\alpha \rightarrow \beta}$ and $\Delta T_{\alpha \rightarrow \beta}$ to find I_β .

Remark: Our work is the first to find that **offset misalignment between image and text modalities in CLIP space depends on concept distance**. In what follows, we design an experiment to show that less offset misalignment leads to a better generative adaptation with directional loss.

3.2. Impact of Offset Misalignment on Generative Model Adaptation

In the previous section, we performed an empirical study that revealed the offset misalignment for natural data. In this section, we take a step further and investigate the effect of this misalignment on the generative model adaptation from a source domain (concept) \mathcal{S} to a target domain (concept) \mathcal{T} . Specifically, following zero-shot generative domain adaptation setup [15], for source domain \mathcal{S} , we assume a pre-trained generator $G_{\mathcal{S}}$ and a text description $T_{\mathcal{S}}$ is available. However, for the target domain, only text description $T_{\mathcal{T}}$ is available. To simulate different degrees of misalignment between source and target, we augment target text to get a set of text descriptions $\{T_{\mathcal{T}}^i\}$. Then, we perform zero-shot adaptation using the directional loss (Eq. 1) from the source domain \mathcal{S} to each of these target text $T_{\mathcal{T}}^i$ and measure the generation performance of adapted generator.

Experimental Setup. For this experiment, we perform adaptation on Human \rightarrow Baby and Dog \rightarrow Cat. We use StyleGAN2-ADA [23] pre-trained on FFHQ [22] and AFHQ-Dog [5] as the pre-trained model. We fix the source text $T_{\mathcal{S}}$ and augment the target text $T_{\mathcal{T}}$ by sampling hand-crafted prompts from the CLIP ImageNet template (INt)¹ which leads to increasing the misalignment (see Supp Sec. C.2 for details). Then, we follow exactly the same hyperparameters as NADA (see Supp Sec. C.3) to adapt the source generator to different target text $T_{\mathcal{T}}^i$. We use FID to mea-

¹https://github.com/openai/CLIP/blob/main/notebooks/Prompt_Engineering_for_ImageNet.ipynb

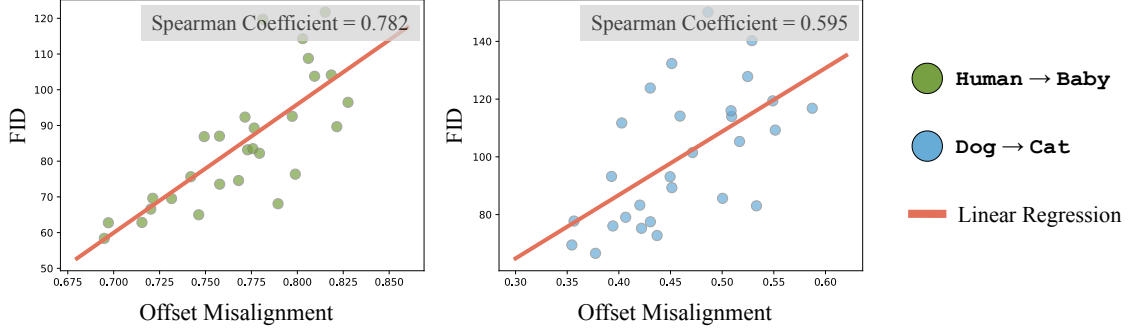


Figure 3. **Impact of offset misalignment on zero-shot generative model adaptation with directional loss:** For each of the two setups, we fix the source domain and augment the text description of the target domain to simulate various degrees of misalignment between image offset and text offset. Then, we perform the adaptation using directional loss in Eq. 1 for each setup. Results show that adaptation performance degrades by increasing the offset misalignment.

sure the performance of the adapted generator against offset misalignment.

Our results in Fig. 3 demonstrates that in general, **increasing the offset misalignment degrades the performance of the zero-shot generative adaption with directional loss.** Motivated by this finding, we propose an approach to iteratively refine the adaptation direction.

4. Methodology: Adaptation with Iterative Refinement

Our analysis in Sec. 3 suggests that for the closer concepts, there is less offset misalignment in CLIP space, resulting in a more accurate directional loss (Eq. 1) for adaptation. Here, we leverage this property to enhance the zero-shot generative model adaptation with directional loss.

Specifically, even though the concept distance between source \mathcal{S} and target \mathcal{T} is fixed, after limited iterations of adaptation using directional loss, the encoded concept in the adapted generator is already closer to the target domain than the encoded concept in source generator (see Supp. Sec. G). For example, when adapting a generator pre-trained on Photo to the target domain Painting, after limited iterations, the adapted generator already encodes some knowledge related to the Painting domain, while this knowledge does not exist in the pre-trained generator.

Therefore, we use the adapted generator as the new anchor (denoted by $G_{\mathcal{A}}$), and compute the directional loss from this anchor point to the target. We update this anchor point iteratively during adaptation, as we move closer to the target domain. Because of the smaller concept distance, our previous analysis suggests that the directional loss computed based on $G_{\mathcal{A}}$ can provide better guidance and rectify the adaptation direction solely computed based on $G_{\mathcal{S}}$. The major challenge of using $G_{\mathcal{A}}$ within directional loss is that related text prompt $P_{\mathcal{A}}$ that describes this concept is unknown. In what follows, first, we discuss the details of the

proposed **Adaptation with Iterative Refinement (AIR)** in Sec. 4.1. Then, to address the challenge of unknown $P_{\mathcal{A}}$ within the directional loss of AIR, we discuss the proposed prompt learning approach in Sec. 4.2.

4.1. Adaptation with Iterative Refinement (AIR)

In our proposed approach, first, we adapt the generator to the target domain for t_{thresh} iterations using directional loss in Eq. 1 to make sure the adapted generator has moved closer to the target domain. Then, in each t_{int} interval of adaptation, we sample the adapted generator as the new anchor point. We denote i^{th} sampled anchor by $G_{\mathcal{A}_i}$. **To reduce offset misalignment and provide more accurate direction, we use the anchor point \mathcal{A}_i instead of source point \mathcal{S} for computing the directional loss.** The proposed AIR scheme is illustrated in Fig. 4 (a). The image offset with anchor point \mathcal{A}_i is computed based on the sampled generator $G_{\mathcal{A}_i}$, and the trainable generator G_t : $\Delta I_{\mathcal{A}_i \rightarrow t} = E_I(G_t(w)) - E_I(G_{\mathcal{A}_i}(w))$. Assuming that the anchor point is described by the prompt $P_{\mathcal{A}_i}$ in the text domain (details of acquiring $P_{\mathcal{A}_i}$ will be discussed in Sec. 4.2), the text offset with anchor point is calculated as follows: $\Delta T_{\mathcal{A}_i \rightarrow \mathcal{T}} = E_T(T_{\mathcal{T}}) - E_T(P_{\mathcal{A}_i})$. Finally, the adaptive loss $\mathcal{L}_{adaptive}$ is computed by aligning the image and text offsets from anchor point \mathcal{A}_i to target \mathcal{T} :

$$\mathcal{L}_{adaptive} = 1 - \cos(\Delta I_{\mathcal{A}_i \rightarrow t}, \Delta T_{\mathcal{A}_i \rightarrow \mathcal{T}}) \quad (3)$$

We empirically find that adding this adaptive loss to $\mathcal{L}_{direction}$ results in a more stable adaptation. The pseudocode can be found in Supp Sec. B.

4.2. Aligning Prompt to Images

Here, we explain the details of the proposed method for learning the text prompt $P_{\mathcal{A}_i}$ that describes the i^{th} anchor point \mathcal{A}_i in text domain. Inspired by [51, 64], we define the prompt $P_{\mathcal{A}_i} \in \mathbb{R}^{(M+1) \times d}$ as combination of M learnable

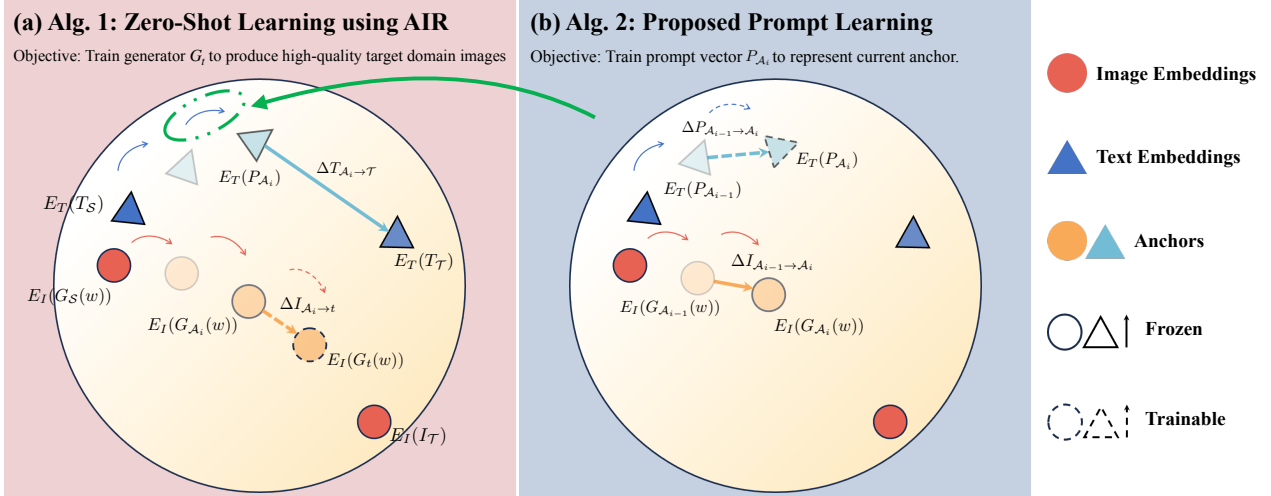


Figure 4. **Illustration of the proposed AIR method:** (a) Zero-shot learning scheme using Adaptation with Iterative Refinement (AIR) (Sec. 4.1). (b) The proposed prompt learning method to learn text embedding $P_{\mathcal{A}_i}$ for the anchor \mathcal{A}_i (Sec. 4.2).

tokens $[V]_j^i \in \mathbb{R}^d$, and a label token $Y_{\mathcal{A}_i} \in \mathbb{R}^d$:

$$P_{\mathcal{A}_i} = [V]_1^i [V]_2^i \dots [V]_M^i [Y_{\mathcal{A}_i}] \quad (4)$$

Early approaches of prompt learning directly learn the learnable tokens $[V]_j^i$ from related images [63, 64]. However, recently, ITI-GEN [59] (proposed for fair text-to-image generation) shows that learning from the offsets is more efficient for capturing the specific attribute of interest. Inspired by this, we learn the anchor text prompt $P_{\mathcal{A}_i}$ by aligning text offset to the image offset. Here, the image offset is calculated between the current and previous anchors: $\Delta I_{\mathcal{A}_{i-1} \rightarrow \mathcal{A}_i} = E_I(G_{\mathcal{A}_i}(w)) - E_I(G_{\mathcal{A}_{i-1}}(w))$. Similarly, the text prompt offset is calculated as follows: $\Delta P_{\mathcal{A}_{i-1} \rightarrow \mathcal{A}_i} = E_T(P_{\mathcal{A}_i}) - E_T(P_{\mathcal{A}_{i-1}})$. Note that the only trainable parameter is the unknown prompt $P_{\mathcal{A}_i}$ which is learned by aligning image and prompt offsets:

$$\mathcal{L}_{align} = 1 - \cos(\Delta I_{\mathcal{A}_{i-1} \rightarrow \mathcal{A}_i}, \Delta P_{\mathcal{A}_{i-1} \rightarrow \mathcal{A}_i}) \quad (5)$$

The proposed prompt learning approach is shown in Fig. 4 (b). We remark that $P_{\mathcal{A}_i}$ is the tokenized text prompt before the CLIP text encoder, and for simplicity, we slightly abuse the notation and use $E_T(P_{\mathcal{A}_i})$ to show CLIP text embedding for anchor \mathcal{A}_i .

Remark: Given that offset misalignment is less for closer concepts, we propose to use the previous anchor point \mathcal{A}_{i-1} as the source to learn the prompt for the i^{th} anchor \mathcal{A}_i . Since consecutive anchor points are close together, the directional loss is more accurate.

Regularizer: We further propose to use the interpolation between tokenized source and target descriptions as anchor label, *i.e.*, $Y_{\mathcal{A}_i} = (1 - p_i)Y_S + p_iY_T$, with p_i denoting the proportion of the training progress until anchor point

\mathcal{A}_i . The label token acts like a regularizer during prompt learning.

We empirically find that using these design choices results in better adaptation with our AIR mechanism compared to learning the prompts directly from generated images by $G_{\mathcal{A}_i}$. More details of the method are summarized in the pseudo-code in Alg. 1 and 2 in Supp. Sec. B.

5. Experiments

In this section, first, we discuss the details of our experimental setup, followed by an evaluation of our proposed prompt learning method. Then, we compare our proposed AIR method with SOTA approaches both qualitatively and quantitatively. Note that we are the first work in the literature to study zero-shot adaptation of the diffusion models. Finally, we conduct an ablation study on the design of our prompt learning strategy.

5.1. Experimental setup

Generative Models. In this work, we implement zero-shot generative model adaptation for both GANs and diffusion models. The implementation details for each type of model is as follows:

- **Zero-Shot Adaptation of GANs.** In this setup, we follow the previous works [15, 19, 21] settings to adapt StyleGAN2-ADA [23] pre-trained on FFHQ [22] and AFHQ-Dog [5] to various target domains.
- **Zero-Shot Adaptation of Diffusion Models.** In this setup, we use Guided Diffusion [10] pre-trained on FFHQ and AFHQ-Dog from P2-Weighting [4] as our source generator. To speedup training, we use DPM-Solver [38] to generate images in 10 steps. To prevent

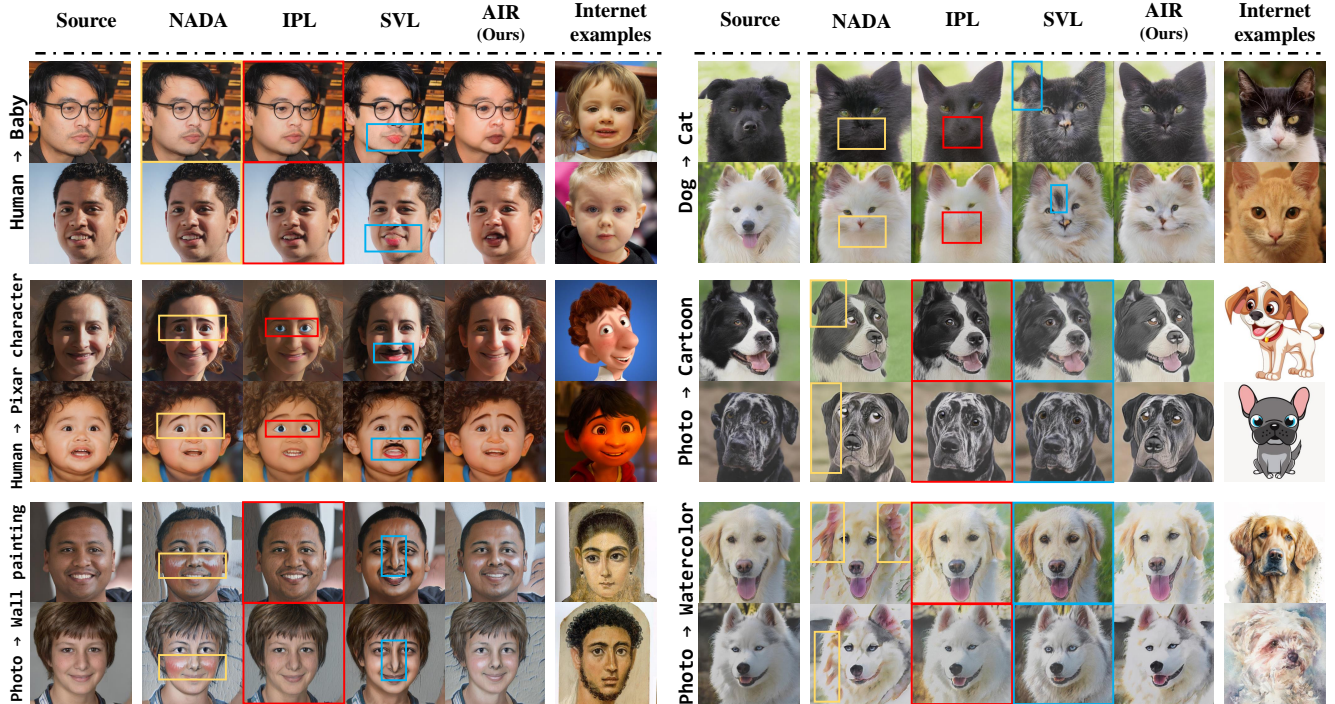


Figure 5. **Qualitative comparison** (Degraded images/regions are highlighted with color boxes). The results of NADA show the adaptation often introduces undesirable changes in features, e.g., missing mouth in Dog \rightarrow Cat, artifacts on ears in Photo \rightarrow Cartoon/Watercolor and red cheeks in Photo \rightarrow Wall painting. For IPL and SVL, a common issue is that the adaptations are inadequate, resulting in images that lack target domain features/styles, especially for adaptations that require drastic feature change, such as Photo \rightarrow Cartoon/Watercolor, etc. Our proposed method does not suffer from artifacts (as shown in target domains Pixar character, Wall painting, and Dog), and adapts better to the style of the target domains, such as Baby, Cartoon and Watercolor. StyleGAN2 is used as pre-trained generator. More qualitative comparisons are shown in Fig. 1 and Supp Sec. A.1. (Best viewed with color and zoom in.)

Table 1. Quantitative evaluation of zero-shot GAN adaptation. Best results are **bold**. For FID, we report only Baby and Cat, which are the only target domains with sufficient samples for reliable FID. Note that compared with previous methods that aim to improve the synthesized sample diversity, our method (AIR) focuses on enhancing the quality of adaptation (lower CLIP Distance and FID), leading to significant gain (e.g. FID improves from 83.29 in IPL to 56.20 in our AIR for distant adaptation Dog \rightarrow Cat). The quality enhancement is consistent for all setups. Furthermore, our method is able to maintain competitive diversity (Intra-LPIPS). Qualitative comparisons of these setups are shown in Fig. 1 and 5.

Pre-trained Dataset	Adaptation	CLIP Distance (\downarrow)				Intra-LPIPS (\uparrow)				FID (\downarrow)			
		NADA	IPL	SVL	AIR	NADA	IPL	SVL	AIR	NADA	IPL	SVL	AIR
FFHQ	Human \rightarrow Baby	0.3327	0.3562	0.3838	0.3325	0.4474	0.4518	0.4506	0.4520	68.35	68.48	158.76	62.13
	Human \rightarrow Pixar	0.2335	0.2343	0.4224	0.2213	0.4759	0.4488	0.4618	0.4717	-	-	-	-
	Photo \rightarrow Wall painting	0.4382	0.4898	0.4952	0.4306	0.4217	0.4320	0.4332	0.4381	-	-	-	-
	Human \rightarrow Werewolf	0.3175	0.2819	0.3868	0.2125	0.4301	0.4387	0.4316	0.4410	-	-	-	-
	Photo \rightarrow Sketch	0.3606	0.3955	0.4092	0.3126	0.4190	0.4292	0.4476	0.4257	-	-	-	-
AFHQ-Dog	Dog \rightarrow Cat	0.1493	0.1530	0.1644	0.1320	0.4439	0.4522	0.4547	0.4628	70.87	83.29	65.79	56.20
	Photo \rightarrow Cartoon	0.2433	0.2419	0.2543	0.2258	0.4356	0.4413	0.4400	0.4427	-	-	-	-
	Photo \rightarrow Watercolor	0.1535	0.1711	0.1646	0.1507	0.4639	0.4703	0.4622	0.4665	-	-	-	-

overfitting, instead of fully fine-tuning the pre-trained model, we fine-tune it with LoRA [20].

During the adaptation of both generators, we utilize the pre-trained ViT-Base/32 [11] as vision encoder for CLIP. Hyperparameter details can be found in Supp. Sec. C.4. *Notably, the only varying hyperparameter for all adaptation setups is the number of adaptation iterations (same as NADA).*

Evaluation Metrics. A well-trained image generator is defined by its ability to produce high-quality and diverse images from target distribution. Following the zero-shot works in literature, we conduct both visual inspections for qualitative evaluations and quantitative evaluations. Specifically, we evaluate image quality with FID and CLIP Distance and measure diversity using Intra-LPIPS [43]. We

introduce additional metrics in Supp. Sec. A.1 to further refine quality assessment. **Additionally, a user study compares image quality and diversity across different schemes based on human feedback.** (See Supp. Sec. C.5 for details.)

5.2. Validate Our Learned Anchor Prompts

To validate our prompt learning, we visualize the learned prompts and generated anchor domain images in CLIP space. As shown in Fig. 6, the prompts accurately represent the anchors (3 of 5 anchors shown for clarity).

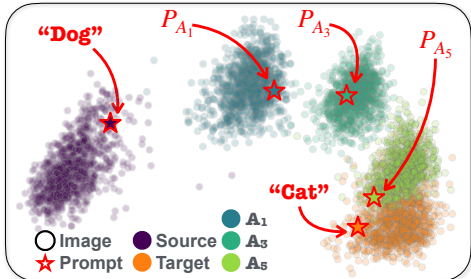


Figure 6. PCA visualization for Dog \rightarrow Cat. For each anchor point \mathcal{A}_i , our learned prompt $P_{\mathcal{A}_i}$ lies within the distribution of 1000 generated images by the generator $G_{\mathcal{A}_i}$ for that anchor point.

5.3. Generative model adaptation

Qualitative results. We report zero-shot GAN adaptation across a wide range of target domains and compare with SOTA methods [15], [19], [21] as shown in Fig. 1 and 5. The results of NADA show the adaptation often introduces undesirable changes in features. For IPL and SVL, the adaptations are inadequate, and resulting images lack target domain feature/style. See discussion in caption for details. Our proposed method can adapt correctly to the target domain. We also show qualitative results of zero-shot diffusion model adaptation in Supp. Sec. A.2, and additional results for GAN adaptation in Supp. Sec. A.1.

Quantitative results. We report FID, Intra-LPIPS, and CLIP Distance to quantify the performance of zero-shot adaptation of both GAN and diffusion model. As shown in Tab. 1 and 4, by mitigating offset misalignment, our method AIR significantly outperforms SOTA methods in quality while maintaining competitive diversity. Our user study results in Tab. 2 further confirm the improvement of our method (see Supp. Sec. K for details).

Additional Experiments. To demonstrate the well-behaved latent space of the pre-trained generator is preserved with our proposed approach, we conduct additional experiments in Supp. More specifically, we perform latent space interpolation (Sec. H), cross-model interpolation (Sec. I), and cross-domain image manipulation (Sec. J). We also conduct an experiment to show our method effectively reduces the offset misalignment (Sec. E).

Table 2. Results of our user study (%) experiments. Note that compared with previous methods that aim to improve diversity, our method focuses on enhancing the quality, and maintain competitive diversity.

Evaluation	NADA	IPL	SVL	AIR
Quality	29.55	3.03	8.33	59.09
Diversity	25.45	32.27	11.83	30.45

Table 3. Ablation study on prompt learning scheme. Visual ablation results can be found in Supp. Sec. D.3.

Methods	Human \rightarrow Baby		Dog \rightarrow Cat	
	FID (\downarrow)	Intra-LPIPS (\uparrow)	FID (\downarrow)	Intra-LPIPS (\uparrow)
NADA	68.35	0.4474	70.87	0.4439
$\mathcal{I} \rightarrow \mathcal{T}$	98.35	0.4308	104.59	0.4452
$\mathcal{S} \rightarrow \mathcal{A}_i$	64.39	0.4503	61.75	0.4630
$\mathcal{A}_{i-1} \rightarrow \mathcal{A}_i$	62.13	0.4520	56.20	0.4628

Table 4. Quantitative evaluation of zero-shot diffusion model adaptation. Note that we report FID only for that target domain Baby, which has a large and publicly available dataset [22]. (More results in Supp. Sec. A.2)

Pre-trained Dataset	Adaptation	CLIP Distance (\downarrow)		Intra-LPIPS (\uparrow)		FID (\downarrow)	
		NADA	AIR	NADA	AIR	NADA	AIR
FFHQ	Human \rightarrow Baby	0.2598	0.2162	0.5700	0.5779	65.54	58.05
	Photo \rightarrow Sketch	0.4405	0.3576	0.4868	0.4860	-	-
AFHQ-Dog	Photo \rightarrow Watercolor	0.1916	0.1848	0.5216	0.5283	-	-
	Photo \rightarrow Cartoon	0.2544	0.2472	0.5574	0.5603	-	-

5.4. Ablation Study

We conduct an ablation study to verify the effectiveness of our prompt learning design, comparing three schemes: i) $\mathcal{I} \rightarrow \mathcal{T}$: We follow IPL to learn a latent mapper that directly produces prompt descriptions from each image. ii) $\mathcal{S} \rightarrow \mathcal{A}_i$: We learn the prompt by capturing the semantic difference between \mathcal{S} and \mathcal{A} with directional loss: $\mathcal{L}_{align}^{\mathcal{S}} = 1 - \cos(\Delta I_{\mathcal{S} \rightarrow \mathcal{A}_i}, \Delta P_{\mathcal{S} \rightarrow \mathcal{A}_i})$. iii) $\mathcal{A}_{i-1} \rightarrow \mathcal{A}_i$: Our proposed prompt learning scheme, which captures the semantic difference between consecutive anchors \mathcal{A}_{i-1} and \mathcal{A}_i with our proposed directional loss in Eq. 5. The results shown in Tab. 3 demonstrate our prompt learning design reduces offset misalignment compared to other schemes, therefore, leading to more accurate prompts and better zero-shot adaptation. Our visual ablation results in Supp. Sec. D.3 further confirm this observation. Additionally, we conduct more ablation studies on hyperparameter selection and token label initialization in Supp. Sec. D.1 and D.2.

6. Conclusion

Previous methods in ZSGM assume that image offset and text offset are perfectly aligned in CLIP embedding space. In this paper, inspired by the studies in analogical reasoning of NLP, we conduct an empirical study to analyze the misalignment between image offset and text offset in CLIP space. Our analysis reveals that there is offset misalignment in CLIP space which correlated with concept

distances. Building on this insight, we propose AIR, a new approach that iteratively samples anchor points closer to the target and mitigates offset misalignment issues. Extensive experimental results shows that the proposed AIR achieves SOTA performance across various setups.

References

- [1] Milad Abdollahzadeh, Touba Malekzadeh, Christopher TH Teo, Keshigeyan Chandrasegaran, Guimeng Liu, and Ngai-Man Cheung. A survey on generative modeling with limited data, few shots, and zero shot. *arXiv preprint arXiv:2307.14397*, 2023. 1, 3
- [2] Yuval Alaluf, Or Patashnik, and Daniel Cohen-Or. Restyle: A residual-based stylegan encoder via iterative refinement. In *Proceedings of the IEEE/CVF International Conference on Computer Vision*, pages 6711–6720, 2021. 23, 24
- [3] Andrew Brock, Jeff Donahue, and Karen Simonyan. Large scale GAN training for high fidelity natural image synthesis. In *7th International Conference on Learning Representations, ICLR 2019, New Orleans, LA, USA, May 6-9, 2019*, 2019. 1
- [4] Jooyoung Choi, Jungbeom Lee, Chaehun Shin, Sungwon Kim, Hyunwoo Kim, and Sungroh Yoon. Perception prioritized training of diffusion models. In *Proceedings of the IEEE/CVF Conference on Computer Vision and Pattern Recognition*, pages 11472–11481, 2022. 6
- [5] Yunjey Choi, Youngjung Uh, Jaejun Yoo, and Jung-Woo Ha. Stargan v2: Diverse image synthesis for multiple domains. In *2020 IEEE/CVF Conference on Computer Vision and Pattern Recognition, CVPR 2020, Seattle, WA, USA, June 13-19, 2020*, pages 8185–8194, 2020. 4, 6, 12, 15, 16, 18, 19, 20
- [6] Trevor Cohen, Dominic Widdows, and Thomas Rindfleisch. Expansion-by-analogy: A vector symbolic approach to semantic search. In *Quantum Interaction*, pages 54–66, 2015. 26
- [7] Ronan Collobert and Jason Weston. A unified architecture for natural language processing: deep neural networks with multitask learning. In *Proceedings of the 25th International Conference on Machine Learning*, page 160–167, 2008. 26
- [8] Joachim Daiber, Lautaro Quiroz, Roger Wechsler, and Stella Frank. Splitting compounds by semantic analogy. In *Proceedings of the 1st Deep Machine Translation Workshop*, pages 20–28, 2015. 26
- [9] Jia Deng, Wei Dong, Richard Socher, Li-Jia Li, Kai Li, and Fei-Fei Li. Imagenet: A large-scale hierarchical image database. In *2009 IEEE Computer Society Conference on Computer Vision and Pattern Recognition (CVPR 2009)*, 20-25 June 2009, Miami, Florida, USA, pages 248–255, 2009. 4
- [10] Prafulla Dhariwal and Alexander Nichol. Diffusion models beat gans on image synthesis. *Advances in neural information processing systems*, 34:8780–8794, 2021. 1, 6, 12, 19
- [11] Alexey Dosovitskiy, Lucas Beyer, Alexander Kolesnikov, Dirk Weissenborn, Xiaohua Zhai, Thomas Unterthiner, Mostafa Dehghani, Matthias Minderer, Georg Heigold, Sylvain Gelly, Jakob Uszkoreit, and Neil Houlsby. An image is worth 16x16 words: Transformers for image recognition at scale. In *9th International Conference on Learning Representations, ICLR 2021, Virtual Event, Austria, May 3-7, 2021*, 2021. 7
- [12] Nguyen Tuan Duc, Danushka Bollegala, and Mitsuru Ishizuka. Cross-language latent relational search between japanese and english languages using a web corpus. In *ACM Transactions on Asian Language Information Processing (TALIP)*, pages 54–66, 2015. 26
- [13] Li Fei-Fei, Rob Fergus, and Pietro Perona. Learning generative visual models from few training examples: An incremental bayesian approach tested on 101 object categories. *Computer vision and Image understanding*, 106(1):59–70, 2007. 4
- [14] Louis Fournier, Emmanuel Dupoux, and Ewan Dunbar. Analogies minus analogy test: measuring regularities in word embeddings. In *Proceedings of the 24th Conference on Computational Natural Language Learning*, pages 365–375, 2020. 2, 26
- [15] Rinon Gal, Or Patashnik, Haggai Maron, Amit H Bermano, Gal Chechik, and Daniel Cohen-Or. Stylegan-nada: Clip-guided domain adaptation of image generators. *ACM Transactions on Graphics (TOG)*, 41(4):1–13, 2022. 1, 3, 4, 6, 8, 18, 20, 23, 25, 28
- [16] Rinon Gal, Yuval Alaluf, Yuval Atzmon, Or Patashnik, Amit Haim Bermano, Gal Chechik, and Daniel Cohen-or. An image is worth one word: Personalizing text-to-image generation using textual inversion. In *The Eleventh International Conference on Learning Representations*, 2023. 20
- [17] Anna Gladkova, Aleksandr Drozd, and Satoshi Matsuoka. Analogy-based detection of morphological and semantic relations with word embeddings: what works and what doesn't. In *Proceedings of the NAACL Student Research Workshop*, pages 8–15, 2016. 26
- [18] Ian J. Goodfellow, Jean Pouget-Abadie, Mehdi Mirza, Bing Xu, David Warde-Farley, Sherjil Ozair, Aaron C. Courville, and Yoshua Bengio. Generative adversarial nets. In *Advances in Neural Information Processing Systems 27: Annual Conference on Neural Information Processing Systems 2014, December 8-13 2014, Montreal, Quebec, Canada*, pages 2672–2680, 2014. 1
- [19] Jiayi Guo, Chaofei Wang, You Wu, Eric Zhang, Kai Wang, Xingqian Xu, Humphrey Shi, Gao Huang, and Shiji Song. Zero-shot generative model adaptation via image-specific prompt learning. In *Proceedings of the IEEE/CVF Conference on Computer Vision and Pattern Recognition*, pages 11494–11503, 2023. 1, 3, 6, 8, 18, 20, 25, 27, 28
- [20] Edward J Hu, Yelong Shen, Phillip Wallis, Zeyuan Allen-Zhu, Yuanzhi Li, Shean Wang, Lu Wang, and Weizhu Chen. LoRA: Low-rank adaptation of large language models. In *International Conference on Learning Representations*, 2022. 7
- [21] Seogkyu Jeon, Bei Liu, Pilhyeon Lee, Kibeom Hong, Jianlong Fu, and Hyeran Byun. Improving diversity in zero-shot gan adaptation with semantic variations. In *Proceedings of the IEEE/CVF International Conference on Computer Vision*, pages 7258–7267, 2023. 1, 3, 6, 8, 18, 20, 25

- [22] Tero Karras, Samuli Laine, and Timo Aila. A style-based generator architecture for generative adversarial networks. In *IEEE Conference on Computer Vision and Pattern Recognition, CVPR 2019, Long Beach, CA, USA, June 16-20, 2019*, pages 4401–4410, 2019. 1, 4, 6, 8, 12, 17, 19, 23
- [23] Tero Karras, Miika Aittala, Janne Hellsten, Samuli Laine, Jaakko Lehtinen, and Timo Aila. Training generative adversarial networks with limited data. In *Advances in Neural Information Processing Systems 33: Annual Conference on Neural Information Processing Systems 2020, NeurIPS 2020, December 6-12, 2020, virtual*, 2020. 4, 6
- [24] Tero Karras, Samuli Laine, Miika Aittala, Janne Hellsten, Jaakko Lehtinen, and Timo Aila. Analyzing and improving the image quality of StyleGAN. In *Proc. CVPR*, 2020. 1, 28
- [25] Tero Karras, Samuli Laine, Miika Aittala, Janne Hellsten, Jaakko Lehtinen, and Timo Aila. Analyzing and improving the image quality of stylegan. In *2020 IEEE/CVF Conference on Computer Vision and Pattern Recognition, CVPR 2020, Seattle, WA, USA, June 13-19, 2020*, pages 8107–8116, 2020. 1
- [26] Leonard Kaufman and Peter J Rousseeuw. *Partitioning Around Medoids (Program PAM)*, chapter 2. John Wiley & Sons, 2009. 20
- [27] Gwanghyun Kim, Taesung Kwon, and Jong Chul Ye. Diffusionclip: Text-guided diffusion models for robust image manipulation. In *Proceedings of the IEEE/CVF Conference on Computer Vision and Pattern Recognition (CVPR)*, pages 2426–2435, 2022. 23, 24
- [28] Maximilian Köper, Christian Scheible, and Sabine Schulte im Walde. Multilingual reliability and “semantic” structure of continuous word spaces. In *Proceedings of the 11th international conference on computational semantics*, pages 40–45, 2015. 2, 26
- [29] Ranjay Krishna, Yuke Zhu, Oliver Groth, Justin Johnson, Kenji Hata, Joshua Kravitz, Stephanie Chen, Yannis Kalantidis, Li-Jia Li, David A Shamma, et al. Visual genome: Connecting language and vision using crowdsourced dense image annotations. *International journal of computer vision*, 123:32–73, 2017. 4
- [30] Alex Krizhevsky, Geoffrey Hinton, et al. Learning multiple layers of features from tiny images.(2009), 2009. 4
- [31] Alina Kuznetsova, Hassan Rom, Neil Alldrin, Jasper Uijlings, Ivan Krasin, Jordi Pont-Tuset, Shahab Kamali, Stefan Popov, Matteo Mallocci, Alexander Kolesnikov, Tom Duerig, and Vittorio Ferrari. The open images dataset v4: Unified image classification, object detection, and visual relationship detection at scale. *IJCV*, 2020. 4
- [32] Gihyun Kwon and Jong Chul Ye. One-shot adaptation of gan in just one clip. *IEEE Transactions on Pattern Analysis and Machine Intelligence*, 2023. 1
- [33] Omer Levy and Yoav Goldberg. Linguistic regularities in sparse and explicit word representations. In *Proceedings of the Eighteenth Conference on Computational Natural Language Learning*, pages 171–180, 2014. 1, 26
- [34] Omer Levy, Yoav Goldberg, and Ido Dagan. Improving distributional similarity with lessons learned from word embeddings. *Transactions of the association for computational linguistics*, 3:211–225, 2015. 2, 26
- [35] Hengjia Li, Yang Liu, Linxuan Xia, Yuqi Lin, Wenxiao Wang, Tu Zheng, Zheng Yang, Xiaohui Zhong, Xiaobo Ren, and Xiaofei He. Few-shot hybrid domain adaptation of image generator. In *The Twelfth International Conference on Learning Representations*, 2024. 1
- [36] Yijun Li, Richard Zhang, Jingwan Lu, and Eli Shechtman. Few-shot image generation with elastic weight consolidation. In *Advances in Neural Information Processing Systems 33: Annual Conference on Neural Information Processing Systems 2020, NeurIPS 2020, December 6-12, 2020, virtual*, 2020. 1
- [37] Tsung-Yi Lin, Michael Maire, Serge Belongie, James Hays, Pietro Perona, Deva Ramanan, Piotr Dollár, and C Lawrence Zitnick. Microsoft coco: Common objects in context. In *Computer Vision—ECCV 2014: 13th European Conference, Zurich, Switzerland, September 6-12, 2014, Proceedings, Part V 13*, pages 740–755. Springer, 2014. 4
- [38] Cheng Lu, Yuhao Zhou, Fan Bao, Jianfei Chen, Chongxuan Li, and Jun Zhu. Dpm-solver: A fast ode solver for diffusion probabilistic model sampling in around 10 steps. *Advances in Neural Information Processing Systems*, 35:5775–5787, 2022. 6
- [39] Tomas Mikolov, Kai Chen, Greg Corrado, and Jeffrey Dean. Efficient estimation of word representations in vector space. In *1st International Conference on Learning Representations, ICLR 2013, 2013*. 1, 26
- [40] Tomas Mikolov, Ilya Sutskever, Kai Chen, Greg S Corrado, and Jeff Dean. Distributed representations of words and phrases and their compositionality. *Advances in neural information processing systems*, 26, 2013. 26
- [41] Tomáš Mikolov, Wen-tau Yih, and Geoffrey Zweig. Linguistic regularities in continuous space word representations. In *Proceedings of the 2013 conference of the north american chapter of the association for computational linguistics: Human language technologies*, pages 746–751, 2013. 1, 26
- [42] Alexander Quinn Nichol and Prafulla Dhariwal. Improved denoising diffusion probabilistic models. In *Proceedings of the 38th International Conference on Machine Learning, ICML 2021, 18-24 July 2021, Virtual Event*, pages 8162–8171, 2021. 1
- [43] Utkarsh Ojha, Yijun Li, Jingwan Lu, Alexei A. Efros, Yong Jae Lee, Eli Shechtman, and Richard Zhang. Few-shot image generation via cross-domain correspondence. In *IEEE Conference on Computer Vision and Pattern Recognition, CVPR 2021, virtual, June 19-25, 2021*, pages 10743–10752, 2021. 1, 7, 18, 20
- [44] Maxime Oquab, Timothée Darcet, Théo Moutakanni, Huy Vo, Marc Szafraniec, Vasil Khalidov, Pierre Fernandez, Daniel Haziza, Francisco Massa, Alaaeldin El-Nouby, et al. Dinov2: Learning robust visual features without supervision. *Transactions on Machine Learning Research Journal*, pages 1–31, 2024. 12
- [45] Or Patashnik, Zongze Wu, Eli Shechtman, Daniel Cohen-Or, and Dani Lischinski. Styleclip: Text-driven manipulation of stylegan imagery. In *2021 IEEE/CVF International Conference on Computer Vision, ICCV 2021, Montreal, QC, Canada, October 10-17, 2021*, pages 2065–2074, 2021. 24

- [46] Jeffrey Pennington, Richard Socher, and Christopher Manning. GloVe: Global vectors for word representation. In *Proceedings of the 2014 Conference on Empirical Methods in Natural Language Processing (EMNLP)*, pages 1532–1543, 2014. [26](#)
- [47] Alec Radford, Jong Wook Kim, Chris Hallacy, Aditya Ramesh, Gabriel Goh, Sandhini Agarwal, Girish Sastry, Amanda Askell, Pamela Mishkin, Jack Clark, Gretchen Krueger, and Ilya Sutskever. Learning transferable visual models from natural language supervision. In *Proceedings of the 38th International Conference on Machine Learning, ICML 2021, 18-24 July 2021, Virtual Event*, pages 8748–8763, 2021. [3](#), [25](#), [28](#)
- [48] Anna Rogers, Aleksandr Drozd, and Bofang Li. The (too many) problems of analogical reasoning with word vectors. In *Proceedings of the 6th Joint Conference on Lexical and Computational Semantics (*SEM 2017)*, pages 135–148, 2017. [2](#), [26](#)
- [49] Robin Rombach, Andreas Blattmann, Dominik Lorenz, Patrick Esser, and Björn Ommer. High-resolution image synthesis with latent diffusion models. In *Proceedings of the IEEE/CVF Conference on Computer Vision and Pattern Recognition*, pages 10684–10695, 2022. [1](#)
- [50] Yujun Shen and Bolei Zhou. Closed-form factorization of latent semantics in gans. In *Proceedings of the IEEE/CVF conference on computer vision and pattern recognition*, pages 1532–1540, 2021. [24](#)
- [51] Christopher TH Teo, Milad Abdollahzadeh, Xinda Ma, and Ngai-man Cheung. Fairqueue: Rethinking prompt learning for fair text-to-image generation. *arXiv preprint arXiv:2410.18615*, 2024. [5](#)
- [52] Omer Tov, Yuval Alaluf, Yotam Nitzan, Or Patashnik, and Daniel Cohen-Or. Designing an encoder for stylegan image manipulation. *ACM Transactions on Graphics (TOG)*, 40(4): 1–14, 2021. [23](#), [24](#), [28](#)
- [53] Joseph Turian, Lev Ratinov, and Yoshua Bengio. Word representations: a simple and general method for semi-supervised learning. In *Proceedings of the 48th annual meeting of the association for computational linguistics*, pages 384–394, 2010. [26](#)
- [54] Ekaterina Vylomova, Laura Rimell, Trevor Cohn, and Timothy Baldwin. Take and took, gaggle and goose, book and read: Evaluating the utility of vector differences for lexical relation learning. In *Proceedings of the 54th Annual Meeting of the Association for Computational Linguistics*, 2015. [26](#)
- [55] Xiyu Wang, Baijiong Lin, Daochang Liu, Ying-Cong Chen, and Chang Xu. Bridging data gaps in diffusion models with adversarial noise-based transfer learning. In *Forty-first International Conference on Machine Learning*, 2024. [1](#)
- [56] Fisher Yu, Ari Seff, Yinda Zhang, Shuran Song, Thomas Funkhouser, and Jianxiong Xiao. Lsun: Construction of a large-scale image dataset using deep learning with humans in the loop. *ArXiv preprint*, abs/1506.03365, 2015. [12](#), [13](#), [14](#)
- [57] Jerrold H Zar. Spearman rank correlation. *Encyclopedia of Biostatistics*, 7, 2005. [4](#), [24](#)
- [58] Xiaohua Zhai, Basil Mustafa, Alexander Kolesnikov, and Lucas Bayer. Sigmoid loss for language image pre-training. In *Proceedings of the IEEE/CVF international conference on computer vision*, pages 11975–11986, 2023. [12](#)
- [59] Cheng Zhang, Xuanbai Chen, Siqi Chai, Henry Chen Wu, Dmitry Lagun, Thabo Beeler, and Fernando De la Torre. ITI-GEN: Inclusive text-to-image generation. In *ICCV*, 2023. [6](#)
- [60] Yunqing Zhao, Keshigeyan Chandrasegaran, Milad Abdollahzadeh, and Ngai-Man Man Cheung. Few-shot image generation via adaptation-aware kernel modulation. *Advances in Neural Information Processing Systems*, 35:19427–19440, 2022. [1](#), [20](#)
- [61] Yunqing Zhao, Henghui Ding, Houjing Huang, and Ngai-Man Cheung. A closer look at few-shot image generation. In *Proceedings of the IEEE/CVF Conference on Computer Vision and Pattern Recognition*, pages 9140–9150, 2022.
- [62] Yunqing Zhao, Chao Du, Milad Abdollahzadeh, Tianyu Pang, Min Lin, Shuicheng Yan, and Ngai-Man Cheung. Exploring incompatible knowledge transfer in few-shot image generation. In *Proceedings of the IEEE/CVF Conference on Computer Vision and Pattern Recognition*, pages 7380–7391, 2023. [1](#), [20](#)
- [63] Kaiyang Zhou, Jingkang Yang, Chen Change Loy, and Ziwei Liu. Conditional prompt learning for vision-language models. In *IEEE/CVF Conference on Computer Vision and Pattern Recognition (CVPR)*, 2022. [6](#), [22](#)
- [64] Kaiyang Zhou, Jingkang Yang, Chen Change Loy, and Ziwei Liu. Learning to prompt for vision-language models. *International Journal of Computer Vision (IJCV)*, 2022. [5](#), [6](#), [22](#)
- [65] Yang Zhou, Zichong Chen, and Hui Huang. Deformable one-shot face stylization via dino semantic guidance. In *Proceedings of the IEEE/CVF Conference on Computer Vision and Pattern Recognition*, pages 7787–7796, 2024. [1](#)
- [66] Jingyuan Zhu, Huimin Ma, Jiansheng Chen, and Jian Yuan. High-quality and diverse few-shot image generation via masked discrimination. *IEEE Transactions on Image Processing*, 2024.
- [67] Peihao Zhu, Rameen Abdal, John Femiani, and Peter Wonka. Mind the gap: Domain gap control for single shot domain adaptation for generative adversarial networks. In *The Tenth International Conference on Learning Representations, ICLR 2022, Virtual Event, April 25-29, 2022*, 2022. [1](#)

Overview

In this supplementary material, we provide additional experiments, ablation studies, and reproducibility details to support our findings. These sections are not included in the main paper due to space constraints.

Contents

A More Experimental Results	12
A.1 Zero-shot GAN Adaptation	12
A.2 Zero-shot Diffusion Model Adaptation	12
B Algorithm	18
C Detailed Experimental Setting	18
C.1. Details of Empirical Analysis	18
C.2. Details of Impact of Offset Misalignment	18
C.3. Hyperparameters of Impact of Offset Misalignment	18
C.4. Hyperparameters of Zero-Shot Adaptation	18
C.5. Evaluation Details	18
D Additional Ablation Studies	21
D.1. Ablation on Hyperparameters Selection	21
D.2. Ablation on Anchor Label Initialization	22
D.3. Visual Ablation Studies	22
E Offset Misalignment Alleviation	22
F Offset Misalignment in more CLIP Space	22
G Concept Shifts during Adaptation	23
H Latent Space Interpolation	23
I. Cross-model Interpolation	23
J. Image Manipulation	23
J.1. GAN-based Image Manipulation	24
J.2. Diffusion-based Image Manipulation	24
K User Study	24
L Related Work	24
MLimitation	27
N Social Impact	28
O Licenses	28

A. More Experimental Results

We include a total of **26** different configurations of zero-shot adaptation in this paper. The experimental setting and evaluation metric follow Sec. 5 in the main paper.

A.1. Zero-shot GAN Adaptation

In this section, we provide additional experimental results including quantitative and qualitative results for different adaptation setups using GAN as the generator and introduce more evaluation metrics.

Qualitatives Results. In Fig. 7 and Fig. 8, we perform zero-shot adaptation of a StyleGAN2 pre-trained on LSUN-Church [56] to four different target domains including Skyscraper, Temple, Sketch and Anime. In Fig. 9 and Fig. 10 we report the zero-shot adaptation of a StyleGAN2 pre-trained on AFHQ-Dog [5] to four different target domains including Hamster, Capybara, Wolf and The Joker. Finally, Fig. 11 shows the quantitative and qualitative results of zero-shot adaptation of a StyleGAN2 pre-trained on FFHQ [22] dataset to two different target domains including Watercolor and A Painting of Ukiyo-e Style. The results show that our approach in general adapts better to the style of the target domain and has better sample quality (please check the caption of each image for more detailed discussion).

Quantitative Results. Quantitative results are reported by computing the CLIP Distance between the embeddings of 5K generated images with each approach and the embedding of the text description of the target domain in CLIP space. As the results show, generated images by proposed AIR has smaller CLIP distance meaning that these images are closer to the target domain compared to images generated by other zero-shot approaches.

Additional Metrics. We further evaluate the quality of the generated images by introducing two additional metrics SigLIP Distance [58] and DINOv2 Distance [44]. Similar to the computation of CLIP Distance, SigLIP and DINOv2 Distance are defined as the cosine distance between the SigLIP/DINOv2 embeddings of collected and generated images. As shown in Tab. 5, the results align with those in the main paper, further support the superiority of our proposed AIR.

A.2. Zero-shot Diffusion Model Adaptation

In this section, we provide more qualitative and quantitative results of zero-shot diffusion model adaptation.

Qualitative Results. Here, we report the qualitative results of zero-shot diffusion model adaptation for the same configuration used in Tab. 4 (main paper). More specifically, we use the pre-trained Guided Diffusion model [10] on two different source domains FFHQ [22] (Fig. 12 Top) and AFHQ-Dog [5] (Fig. 12 Bottom) and shift these pre-trained models to different target domains using only text descriptions for both NADA and our proposed AIR approaches. As illustrated in Fig. 12, the generated images with NADA suffer from degradation in the form of artifacts compared to our proposed AIR approach.

More Quantitative Results. We present some addi-

	Source	NADA	IPL	SVL	AIR (Ours)	Internet examples
Church → Skyscraper						
	CLIP Distance (↓)	0.3860	0.3441	0.4209	0.3270	
Church → Temple						
	CLIP Distance (↓)	0.3197	0.3632	0.3177	0.3146	

Figure 7. **Additional zero-shot adaptation results from source domain Church.** Here we use a StyleGAN2 generator pre-trained on the LSUN-Church [56] dataset as G_S and shift this to various target domains using different zero-shot approaches. We report both quantitative and qualitative results for two setups: Church→Skyscraper and Church→Temple. We compute CLIP Distance on 5K generated samples as quantitative results, and as one can see, for both setups, our proposed AIR approach results in less CLIP Distance meaning that the generated images are closer to the target domain. Additionally, qualitative results show that in general our proposed method adapts better to the target domain and has better quality. For example, in line 2 of Church→Skyscraper, NADA and IPL samples contain artifacts around windows, and SVL still has some structures related to the church like the arch in the middle of the skyscraper.

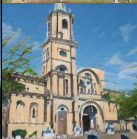
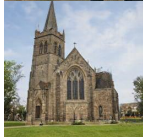
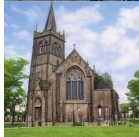
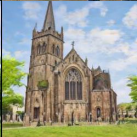
	Source	NADA	IPL	SVL	AIR (Ours)	Internet examples
Photo → Sketch						
						
						
						
	CLIP Distance (↓)	0.2948	0.3070	0.3401	0.2805	
Photo → Anime						
						
						
						
	CLIP Distance (↓)	0.2067	0.2180	0.3503	0.1990	

Figure 8. **Additional zero-shot adaptation results from source domain Church.** Here we use a StyleGAN2 generator pre-trained on the LSUN-Church [56] dataset as G_S and shift this to various target domains using different zero-shot approaches. We report both quantitative and qualitative results for two setups: Photo→Sketch and Photo→Anime. We compute CLIP Distance on 5K generated samples as quantitative results, and as one can see, for both setups, our proposed AIR approach results in less CLIP Distance meaning that the generated images are closer to the target domain. Additionally, qualitative results show that in general our proposed method adapts better to the target domain and has better quality. For example, for Photo→Sketch setup, generated samples with our AIR approach have a more similar style to the target domain.

	Source	NADA	IPL	SVL	AIR (Ours)	Internet examples
Dog → Hamster						
						
						
						
	CLIP Distance (↓)	0.1616	0.1457	0.1826	0.1306	
Dog → Capybara						
						
						
						
	CLIP Distance (↓)	0.1359	0.1446	0.1861	0.1121	

Figure 9. **Additional zero-shot adaptation results from source domain Dog.** Here we use a StyleGAN2 generator pre-trained on the AFHQ-Dog [5] dataset as G_S and shift this to various target domains using different zero-shot approaches. We report both quantitative and qualitative results for two setups: Dog→Hamster and Dog→Capybara. We compute CLIP Distance on 5K generated samples as quantitative results, and as one can see, for both setups, our proposed AIR approach results in less CLIP Distance meaning that the generated images are closer to the target domain. Additionally, qualitative results show that in general our proposed method adapts better to the target domain and has better quality. For example, for Dog→Capybara setup, generated samples with other approaches have degradations like unsymmetrical faces or eyes.

	Source	NADA	IPL	SVL	AIR (Ours)	Internet examples
Dog → Wolf						
						
						
						
	CLIP Distance (↓)	0.1480	0.1519	0.2249	0.1421	
Dog → The Joker						
						
						
						
	CLIP Distance (↓)	0.3708	0.3827	0.4574	0.3131	

Figure 10. **Additional zero-shot adaptation results from source domain Dog.** Here we use a StyleGAN2 generator pre-trained on the AFHQ-Dog [5] dataset as G_S and shift this to various target domains using different zero-shot approaches. We report both quantitative and qualitative results for two setups: Dog→Wolf and Dog→The Joker. We compute CLIP Distance on 5K generated samples as quantitative results, and as one can see, for both setups, our proposed AIR approach results in less CLIP Distance meaning that the generated images are closer to the target domain. Additionally, qualitative results show that in general our proposed method adapts better to the target domain and has better quality. For example, for Dog→Wolf setup, IPL generates an unnaturally big snout and SVL has some artifacts in the generated sample. For Dog→The Joker setup, our approach attains the mouth feature with a proper style and quality.

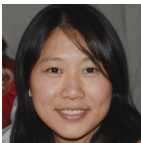
	Source	NADA	IPL	SVL	AIR (Ours)	Internet examples
Photo → Watercolor						
						
						
						
	CLIP Distance (↓)	0.3548	0.3621	0.3639	0.3376	
Photo → A painting of Ukiyo-e Style						
						
						
						
	CLIP Distance (↓)	0.2437	0.2467	0.3906	0.2315	

Figure 11. **Additional zero-shot adaptation results from source domain FFHQ.** Here we use a StyleGAN2 generator pre-trained on the FFHQ [22] (human faces) dataset as G_S and shift this to various target domains using different zero-shot approaches. We report both quantitative and qualitative results for two setups: Photo→Watercolor and Photo→A Painting of Ukiyo-e Style. We compute CLIP Distance on 5K generated samples as quantitative results, and as one can see, for both setups, our proposed AIR approach results in less CLIP Distance meaning that the generated images are closer to the target domain. Additionally, qualitative results show that in general our proposed method adapts better to the target domain and has better quality.

Table 5. Additional quantitative evaluation of zero-shot GAN adaptation, with the same setting of Tab. 1 in main paper.

Pre-trained Dataset	Target Domain	SigLIP Distance (\downarrow)				DINOv2 Distance (\downarrow)			
		NADA	IPL	SVL	AIR	NADA	IPL	SVL	AIR
FFHQ	Baby	0.1925	0.1884	0.3474	0.1833	0.5943	0.5993	0.8026	0.5887
	Werewolf	0.3192	0.3930	0.4831	0.2274	0.8500	0.8923	0.9365	0.7097
	Pixar	0.2803	0.2762	0.4582	0.2630	0.6935	0.6690	0.7848	0.6785
	Sketch	0.2897	0.3173	0.3598	0.2837	0.4682	0.5918	0.6291	0.4420
	Wall painting	0.4205	0.4277	0.4489	0.4103	0.7256	0.7267	0.7836	0.7004
AFHQ-Dog	Cat	0.1395	0.2287	0.1819	0.1297	0.8553	0.8737	0.8842	0.8338
	Cartoon	0.2580	0.2618	0.3140	0.2518	0.7899	0.8174	0.9078	0.7644
	Watercolor	0.1934	0.1980	0.2569	0.1819	0.8059	0.8328	0.8330	0.7943

tional setups for the quantitative evaluation of zero-shot diffusion model adaptation in Tab. 6. Specifically, we report FID, Intra-LPIPS, and CLIP Distance to quantify the performance. Our method consistently outperforms NADA in quality and shows comparable performance in diversity.

B. Algorithm

We provide the pseudo-code of the proposed method in this section. Specifically, we show zero-shot generative model using Adaptation with Iterative Refinement (AIR) in Alg. 1, and our proposed prompt learning scheme in Alg. 2.

C. Detailed Experimental Setting

C.1. Details of Empirical Analysis

For datasets with a single class label for each image, such as ImageNet, Caltech-101, and CIFAR-100, we use the original images from the dataset. For datasets with multiple objects in an image, such as OpenImages, MS COCO, and Visual Genome, to better align with the setting in NADA, we extract the objects using bounding boxes and classify them into their labeled classes.

For a certain concept α , we use the images of the class as I_α . For text description T_α , we use the corresponding class label with INt, e.g., "a photo of a [cat]" when $\alpha = \text{cat}$.

C.2. Details of Impact of Offset Misalignment

We randomly sample prompt template from INt, and perform zero-shot adaptation with NADA as shown in Fig. 3 in main paper. We list the details of the sampled prompts and their offset misalignment \mathcal{M} as well as the adaptation quality (measured by FID) in Tab. 7.

C.3. Hyperparameters of Impact of Offset Misalignment

For the hyperparameter choices in Sec. 3.2, we strictly follow the settings in NADA except that only the ViT-B/32 is used as vision encoder. The details of hyperparameters are shown in Tab. 8.

C.4. Hyperparameters of Zero-Shot Adaptation

In Alg. 1, for both GAN and diffusion model adaptation the batch size is set to 2. Adaptation iteration t_{adapt} is set to 200 for in-domain changes like Human \rightarrow Baby, 300 for texture-based changes such as Photo \rightarrow Sketch, and 2,000 for animal changes like Dog \rightarrow Cat. We set $t_{thresh} = 50\%t_{adapt}$ to ensure there are some target domain concept encoded in G_t , and $t_{int} = 10\%t_{adapt}$ to facilitate a stable and efficient training.

In Alg. 2, we generate 1,000 pairs of source and anchor images with the same batch of w for each update. The number of prompt vectors m is set to 4, and is initialized by "A photo of a". Each of the prompt learning sessions requires $k_{iter} = 200$ iterations.

For all experiments, we use an ADAM optimizer with a learning rate of 0.002 for both Alg.1 and 2. We conduct all the experiments on a single NVIDIA RTX 6000 Ada GPU. The training time is comparable to NADA as prompt learning in Alg. 2 only requires ~ 20 seconds in our environment.

It is important to note that the only varying hyperparameter for all 26 setups is the number of adaptation iterations (same as NADA), and our results show this generalizes well across scenarios.

C.5. Evaluation Details

A well-trained image generator is defined by its ability to produce high-quality and diverse images from target distribution. We follow existing zero-shot works in evaluation setup when applicable, and further improve on them. Specifically, following previous works [15, 19, 21], we have conducted comparisons on both public datasets and images collected from the internet. Our evaluations include both visual inspections for qualitative evaluations and quantitative evaluations using the following metrics:

- **FID.** For target domains with large and publicly available datasets, we follow previous work [21] to use FFHQ-Baby [43] (for target domain Baby), and AFHQ-Cat [5] (for target domain Cat) as target distribution. Then, we generate 5000 samples for each target

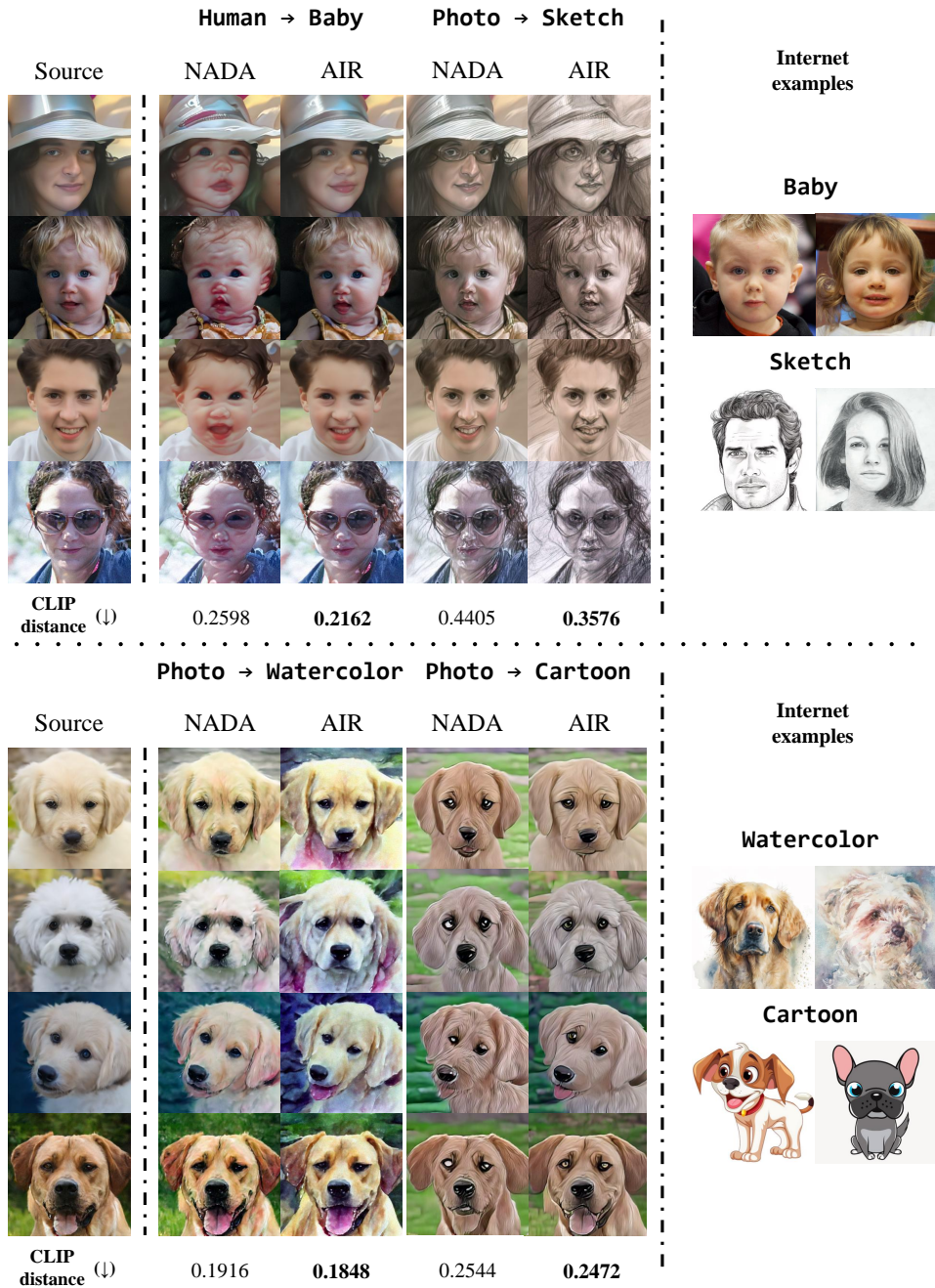


Figure 12. **Additional zero-shot adaptation results.** **Top:** We use a pre-trained Guided Diffusion model [10] on FFHQ dataset [22] as pre-trained generator G_S and perform zero-shot adaptation in two different setups: Human→Baby and Photo→Sketch using both NADA and our proposed AIR approach. Quantitative results measured by CLIP distance show that the generated images by our approach are closer to the target domain. In addition, qualitative results show that NADA suffers from degradation. **Bottom:** We use a pre-trained Guided Diffusion model [10] on AFHQ-Dog dataset [5] as pre-trained generator G_S and perform zero-shot adaptation in two different setups: Photo→Watercolor and Photo→Cartoon using both NADA and our proposed AIR approach. Similarly, both quantitative and qualitative results show that our proposed AIR approach has better performance compared to NADA.

Table 6. More quantitative evaluation of zero-shot diffusion model adaptation. Instead of aiming to improve the synthesized sample diversity, our method focuses on enhancing the quality of adaptation. Note that we report FID only for that target domain Baby and Cat, which have large and publicly available datasets for FID computation [5].

Pre-trained Dataset	Adaptation	CLIP Distance (\downarrow)		Intra-LPIPS (\uparrow)		FID (\downarrow)	
		NADA	AIR	NADA	AIR	NADA	AIR
FFHQ	Human \rightarrow Baby	0.2598	0.2162	0.5700	0.5779	65.54	58.05
	Human \rightarrow Werewolf	0.2782	0.2318	0.5208	0.5195	-	-
	Human \rightarrow Pixar characters	0.4316	0.3881	0.4585	0.4549	-	-
	Photo \rightarrow Sketch	0.4405	0.3576	0.4868	0.4860	-	-
	Photo \rightarrow Wall painting	0.4791	0.4771	0.5259	0.5283	-	-
AFHQ-Dog	Dog \rightarrow Cat	0.1406	0.1402	0.5423	0.5445	85.02	77.61
	Photo \rightarrow Cartoon	0.2544	0.2472	0.5574	0.5603	-	-
	Photo \rightarrow Watercolor	0.1916	0.1848	0.5216	0.5283	-	-

Algorithm 1: Zero-Shot Learning using Adaptation with Iterative Refinement (AIR)

Require: Pre-trained generator G_S , textual descriptions T_S and T_T , t_{adapt} , t_{thresh} , t_{int} , learning rate η , CLIP image and text encoder E_I and E_T

Output: Trained generator G_t to produce high-quality target domain images

- 1 Initialize G_t by weights of G_S and freeze weights of G_S , $i = 0$, $\mathcal{L}_{adaptive} = 0$
- 2 $\Delta T_{S \rightarrow T} = E_T(T_T) - E_T(T_S)$
- 3 **for** $t = 0$; $t++$; $t < t_{adapt}$ **do**
- 4 $\Delta I_{S \rightarrow t} = E_I(G_t(w)) - E_I(G_S(w))$
- 5 $\mathcal{L}_{direction} = 1 - \cos(\Delta I_{S \rightarrow t}, \Delta T_{S \rightarrow T})$
- 6 **if** $t \% t_{int} = 0$ **then**
- 7 $i++$
- 8 $G_{A_i} = G_t$
- 9 $P_{A_i} = \text{Prompt-Learning}(G_{A_i}, G_{A_{i-1}}, P_{A_{i-1}})$ /* refer to Algorithm 2 for details */
- 10 **end**
- 11 **if** $t > t_{thresh}$ **then**
- 12 $\Delta I_{A_i \rightarrow t} = E_I(G_t(w)) - E_I(G_{A_i}(w))$ /* if $G_t = G_{A_i}$, add perturbation to $G_t(w)$ */
- 13 $\Delta T_{A_i \rightarrow T} = E_T(T_T) - E_T(P_{A_i})$
- 14 $\mathcal{L}_{adaptive} = 1 - \cos(\Delta I_{A_i \rightarrow t}, \Delta T_{A_i \rightarrow T})$
- 15 **end**
- 16 $\mathcal{L} = \mathcal{L}_{direction} + \mathcal{L}_{adaptive}$
- 17 Update $G_t \leftarrow G_t - \eta \nabla_{G_t} \mathcal{L}$
- 18 **end**

domain [60, 62], and use FID to evaluate the generated images’ quality and diversity.

- **CLIP Distance.** The public data is scarce for other target domains, *e.g.*, Pixar. For these domains, we follow IPL’s idea [19] to collect internet images as reference. However, since IPL did not make the collected images publicly available, we had to repeat the same practice and collect the images. Then, we use the CLIP Distance [16] which is defined as the cosine distance between the clip embeddings of the collected images and the generated images to measure the similarity of the generated images to the target domain.
- **Intra-LPIPS.** To measure the diversity of the generated images, we use Intra-LPIPS metric [43] which first as-

signs generated images to one of K clusters, then averages pair-wise distance within the cluster members and reports the average value over K clusters. In zero-shot setup, since there are no training images, we follow [15, 21] to cluster around generated images using K -Medoids [26], with $K = 10$.

- **User Study.** We also conducted a user study to compare the quality and the diversity of the generated images with different schemes based on human feedback. See more details in Sec. K.

We remark that similarly NADA reports Intra-LPIPS on AFHQ-Cat, and SVL reports both FID and Intra-LPIPS on AFHQ-Cat. In addition, we believe the included visual results can help in transparency and reflecting the superior

Algorithm 2: Proposed Prompt Learning

Require: Current and previous anchor generators $G_{\mathcal{A}_i}$ and $G_{\mathcal{A}_{i-1}}$, learned text prompt for previous anchor $P_{\mathcal{A}_{i-1}}$, learning rate μ , CLIP image and text encoder E_I and E_T

Output: Prompt vector $P_{\mathcal{A}_i}$ to represent current anchor.

```
1  $\Delta I_{\mathcal{A}_{i-1} \rightarrow \mathcal{A}_i} = E_I(G_{\mathcal{A}_i}(w)) - E_I(G_{\mathcal{A}_{i-1}}(w))$ 
2 for  $k = 0; k++; k < k_{iter}$  do
3    $\Delta P_{\mathcal{A}_{i-1} \rightarrow \mathcal{A}_i} = E_T(P_{\mathcal{A}_i}) - E_T(P_{\mathcal{A}_{i-1}})$ .
4    $\mathcal{L}_{align} = 1 - \cos(\Delta I_{\mathcal{A}_{i-1} \rightarrow \mathcal{A}_i}, \Delta P_{\mathcal{A}_{i-1} \rightarrow \mathcal{A}_i})$ 
5   Update  $P_{\mathcal{A}_i} \leftarrow P_{\mathcal{A}_i} - \mu \nabla_{P_{\mathcal{A}_i}} \mathcal{L}_{align}$ 
6 end
```

Table 7. Prompt templates used in Sec. 3.2.

Prompts	Human→Baby		Dog→Cat	
	Offset Misalignment	FID	Offset Misalignment	FID
A bad photo of a { }.	0.6971	62.76	0.3545	69.47
A sculpture of a { }.	0.7895	68.08	0.4713	101.49
A photo of the hard to see { }.	0.7989	76.36	0.4219	75.24
A low resolution photo of the { }.	0.7729	83.18	0.3942	76.06
A rendering of a { }.	0.7577	73.56	0.4028	111.74
Graffiti of a { }.	0.7715	92.34	0.5332	83.03
A bad photo of the { }.	0.7202	66.58	0.3774	66.58
A cropped photo of the { }.	0.8215	89.66	0.4512	132.33
A tattoo of a { }.	0.8060	108.78	0.5490	119.40
The embroidered { }.	0.8185	104.13	0.5514	109.27
A photo of a hard to see { }.	0.7680	74.58	0.4066	79.07
A bright photo of a { }.	0.7315	69.54	0.4305	77.50
A dark photo of the { }.	0.7758	83.50	0.4592	114.12
A drawing of a { }.	0.7765	89.28	0.4304	123.84
A photo of my { }.	0.6949	58.39	0.3566	77.76
The plastic { }.	0.7812	119.73	0.5092	113.99
A photo of the cool { }.	0.8094	103.78	0.4496	93.12
A close-up photo of a { }.	0.7213	69.61	0.4370	72.75
A black and white photo of the { }.	0.7463	64.99	0.5288	140.25
A painting of the { }.	0.8152	121.74	0.4862	150.15
A painting of a { }.	0.7576	87.01	0.4513	89.32
A pixelated photo of the { }.	0.7154	62.85	0.5168	105.32
A sculpture of the { }.	0.7794	82.22	0.5086	115.97
A bright photo of the { }.	0.8029	114.31	0.4203	83.28
A cropped photo of a { }.	0.7493	86.87	0.3929	93.22
A plastic { }.	0.7420	75.65	0.5247	127.82
A photo of the dirty { }.	0.8276	96.47	0.5004	85.62
A jpeg corrupted photo of a { }.	0.7972	92.56	0.5872	88.73

performance of our proposed method in terms of adaptation quality.

D. Additional Ablation Studies

D.1. Ablation on Hyperparameters Selection

We conduct an ablation study to determine the optimal hyperparameters. Specifically, Tab. 9 shows the ablation

Table 8. Hyperparameters choices of NADA in Sec. 3.2.

Source	Target	Prompt template	Iterations	Adaptive k
Human	Baby	INt	300	18
Dog	Cat	INt	2000	3

results for the adaptation interval t_{int} to update anchor. Tab. 10 shows the ablation results for the starting iteration t_{thresh} of applying AIR. A large t_{int} which results in fewer updates of the anchor point, generally leads to a degradation in performance due to less precise adaptation. Conversely, a small t_{int} , while more computationally expensive, does not yield significant improvement. Thus, we set $t_{int} = 10\%$ to balance the computation cost and adaptation precision. Similarly, neither excessively large nor small values of t_{thresh} provide optimal adaptation performance. As shown in Fig. 13 (b) and (c), the visual ablation results align with this conclusion. Hence, we empirically select $t_{thresh} = 50\%$. It is important to note that the only varying hyperparameter for all 26 setups is the number of adaptation iterations (same as NADA), and our results show this generalizes well across scenarios.

Table 9. Ablation study on adaptation interval t_{int} to update anchor.

% of t_{adapt}	t_{int}			
	Human \rightarrow Baby		Dog \rightarrow Cat	
	FID (\downarrow)	Intra-LPIPS (\uparrow)	FID (\downarrow)	Intra-LPIPS (\uparrow)
5%	59.45	0.4512	59.97	0.4560
10%	62.13	0.4520	56.20	0.4628
15%	58.87	0.4515	61.92	0.4635
20%	64.54	0.4496	65.49	0.4537
25%	56.69	0.4511	67.49	0.4374
30%	76.39	0.4506	77.23	0.4513

Table 10. Ablation study on starting iteration t_{thresh} of applying AIR.

% of t_{adapt}	t_{thresh}			
	Human \rightarrow Baby		Dog \rightarrow Cat	
	FID (\downarrow)	Intra-LPIPS (\uparrow)	FID (\downarrow)	Intra-LPIPS (\uparrow)
0%	63.56	0.4324	83.33	0.4815
12.5%	75.92	0.4259	78.21	0.4642
25.0%	72.17	0.4386	73.65	0.4516
37.5%	64.14	0.4558	59.96	0.4496
50.0%	62.13	0.4520	56.20	0.4628
67.5%	68.25	0.4542	56.46	0.4344

D.2. Ablation on Anchor Label Initialization

Our prompt initialization in Sec. 4.2 is inspired by the standard prompt learning in VLM [64] [63], which initializes label token Y with class label of the image to serve as prior.

Table 11. Ablation study on initialization of $Y_{\mathcal{A}_i}$, using: a) Target domain label; b) Source domain label for the first half of adaptation, then target domain label; c) Interpolation as in our AIR.

Init.	Human \rightarrow Baby		Dog \rightarrow Cat	
	FID (\downarrow)	Intra-LPIPS (\uparrow)	FID (\downarrow)	Intra-LPIPS (\uparrow)
a)	67.53	0.4513	65.83	0.4373
b)	63.34	0.4512	56.44	0.4466
c)	62.13	0.4520	56.20	0.4628

Table 12. Offset misalignment between adaptation directions and the ground truth. Note that IPL and SVL have multiple directions.

Adaptation	NADA	IPL	SVL	AIR
Human \rightarrow Baby	0.67	0.69 \pm 0.09	0.92 \pm 0.03	0.49
Dog \rightarrow Cat	0.54	0.65 \pm 0.06	0.59 \pm 0.11	0.25

However, in our setting, the anchor domain encodes both source and target concepts, so it cannot be described with natural language. Therefore, we leverage the continuous and semantically rich embedding space of the text encoder to initialize anchor label $Y_{\mathcal{A}_i}$ via **interpolation** between tokenized source and target descriptions. We conduct an ablation study on the initialization of $Y_{\mathcal{A}_i}$. Results shown in Tab. 11 indicate the effectiveness of our idea by obtaining the best FID and Intra-LPIPS.

D.3. Visual Ablation Studies

We perform visual ablation studies on prompt learning design and hyperparameters selection with the same experiments setting of Sec. 5.4 and D.1. The results in Fig. 13 align consistently with the quantitative findings.

E. Offset Misalignment Alleviation

We demonstrate AIR alleviates the offset misalignment, i.e., our refined direction aligns more with ground truth in Tab. 12. The ground truth is computed by $\Delta I_{S \rightarrow \mathcal{T}} = E_I(\overline{I_{\mathcal{T}}}) - E_I(\overline{G_S(w)})$ (for AIR, the ground truth is $\Delta I_{\mathcal{A}_i \rightarrow \mathcal{T}}$ of the last \mathcal{A}_i), where $I_{\mathcal{T}}$ are real images.

F. Offset Misalignment in more CLIP Space

In this section, we present an additional empirical analysis of offset misalignment to further demonstrate that it is a general property within the CLIP space. Following the experimental setup in Sec. 3.1, but replacing the CLIP ViT-Base/32 vision encoder with CLIP RN50x64, we plot the offset misalignment against concept distance for six public datasets in Fig. 14. Our results demonstrate a consistent and meaningful correlation between offset misalignment and concept distance across different CLIP spaces.

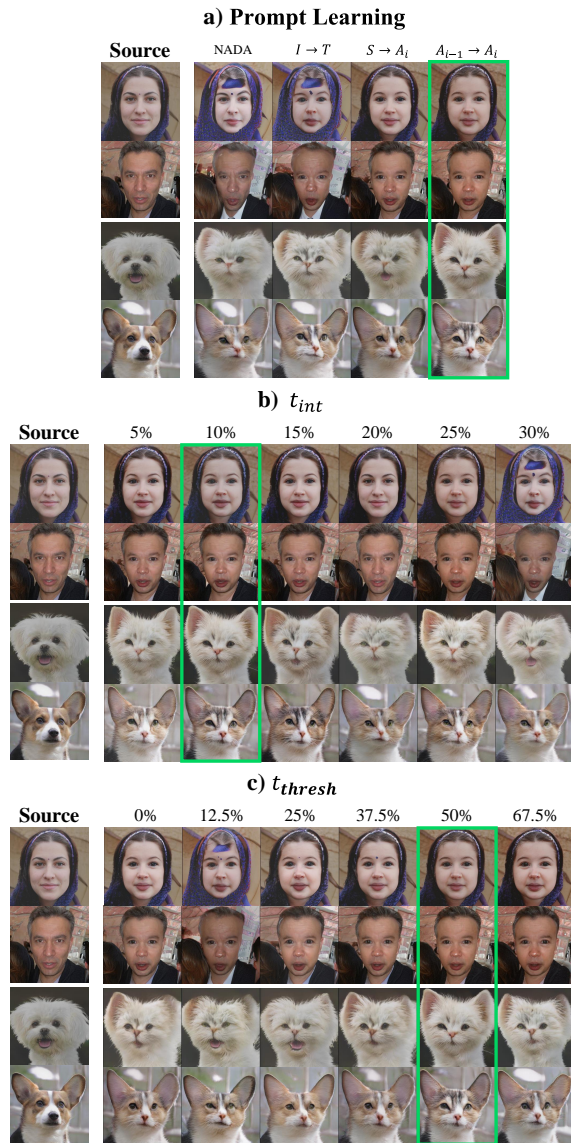


Figure 13. Visual ablation study of: a) Design choice of prompt learning; b) Adaptation interval t_{int} to update anchor; c) Starting iteration t_{thresh} of applying AIR.

G. Concept Shifts during Adaptation

The intuition of our proposed method is that after limited iterations of adaptation using directional loss, the encoded concept in the adapted generator is already closer to the target domain than the encoded concept in source generator. In this section, we design an experiment to demonstrate that the adapted generator already encodes some knowledge related to the target domain. Specifically, following zero-shot generative model domain adaptation setup [15], we perform adaptation on Human \rightarrow Baby with StyleGAN2-ADA pre-

trained on FFHQ [22]. We report FID score throughout the adaptation process to measure the knowledge related to target domain encoded in the adapted generator. Our results in Fig. 15 support our statement. Additionally, we present qualitative results using the same latent code to further support our findings.

H. Latent Space Interpolation

Building on prior research, we demonstrate that the target domain generators refined through our method retain a smooth latent space property. As illustrated in Fig. 16, each row features a series of images from the same target domain. The left-most and right-most images in each row, labeled as $G_t(w_1)$ and $G_t(w_2)$ respectively, are generated using distinct latent codes w_1 and w_2 . Latent space interpolation between these codes produces an image $G_t((1-\gamma)w_1 + \gamma w_2)$, where α varies from 0 to 1. The visual results show that our method has good robustness and generalization ability. The various target domain spaces obtained by our method are consistently smooth.

I. Cross-model Interpolation

In addition to demonstrating latent space interpolation, we also explore the model’s weight smoothness across various domains. Specifically, we perform linear interpolation in the weight space between $G(\cdot, \theta_s)$ and $G(\cdot, \theta_{t_1})$, or between $G(\cdot, \theta_{t_1})$ and $G(\cdot, \theta_{t_2})$. Here, $G(\cdot, \theta_s)$ represents the source domain generator, while $G(\cdot, \theta_{t_1})$ and $G(\cdot, \theta_{t_2})$ are generators adapted to two different target domains. Given a latent code w , we produce images via an interpolated model, $G(w, (1-\gamma)\theta_1 + \gamma\theta_2)$, where γ ranges from 0 to 1. As illustrated in Fig. 17, our approach effectively supports smooth cross-model interpolation, whether transitioning from a source to a target domain or between different target domains.

J. Image Manipulation

To further demonstrate the effectiveness of our proposed method, we also conduct experiments on text-to-image manipulation. It first inverts a image to the latent code by a pre-trained inversion model and then feeds it to the trained target domain generator to get the translated target domain image.

We experiment on both GAN and diffusion model. We use Restyle [2] with e4e encoder [52] to invert a real image into the latent space w for StyleGANs. For the diffusion model, we follow the setting of DiffusionCLIP [27] to diffuse a real image and finetune the model to generate an image with target domain features using the diffused image.

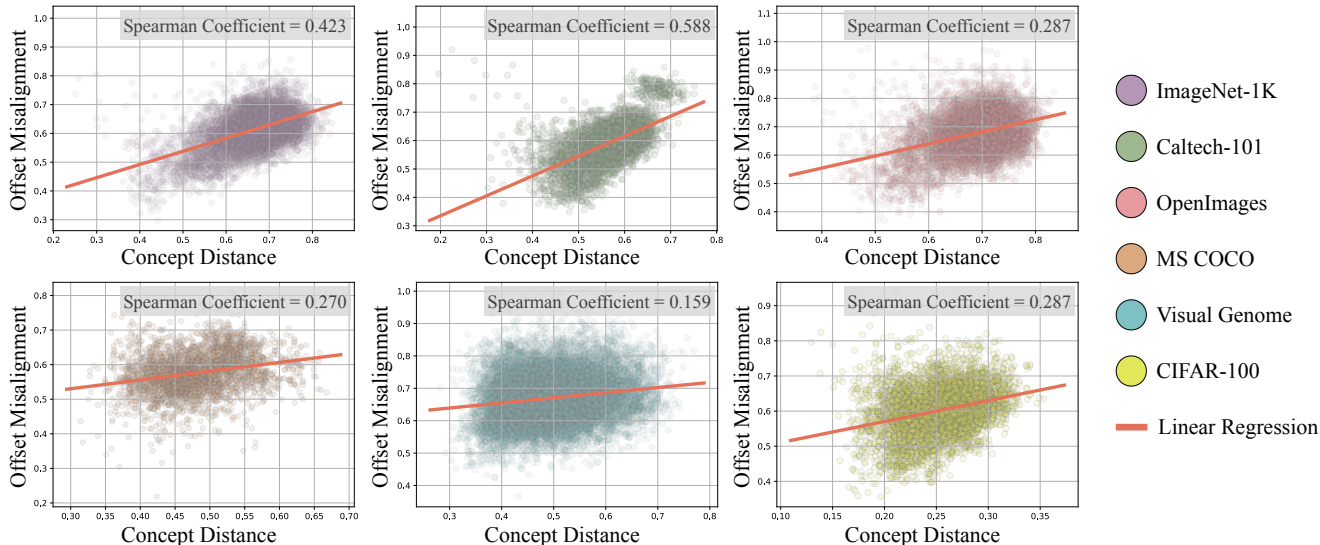


Figure 14. Empirical analysis of offset misalignment in CLIP RN50x64 space. Experiment setup are the same as Sec. 3.1 except that CLIP RN50x64 is used as the vision encoder. Our results show that the meaningful correlation (measured by Spearman’s coefficient [57]) between offset misalignment and concept distance consistently exists in both CNN-based and ViT-based CLIP vision encoders.

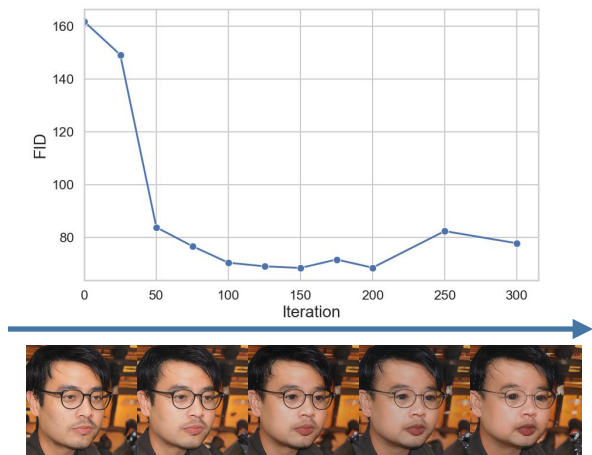


Figure 15. Concept shifts during adaptation.

J.1. GAN-based Image Manipulation

For GAN-based generators, we perform the experiment by utilizing the inversion model Restyle [2] with e4e encoder [52]. As illustrated in Fig 18, our method qualitatively exhibits a higher fidelity of target domain features compared to previous methods. Quantitatively, our approach more closely aligns with the reference target images in CLIP space, indicating a greater semantic similarity.

J.2. Diffusion-based Image Manipulation

We implement based on Diffusion-CLIP [27] which seamlessly integrates with the existing zero-shot adaptation methods.

As illustrated in Fig 19, our method qualitatively exhibits a higher fidelity of target domain feature compared to previous methods. Quantitatively, our approach more closely aligns with the reference target images in CLIP space, indicating a greater semantic similarity.

Fig. 20 illustrates real-world image manipulation results for diffusion AIR.

K. User Study

We conduct a user study to compare the quality and the diversity of the generated images with different schemes based on human feedback. The questionnaire is performed using the generated images by different schemes including NADA, IPL, SVL, and our proposed AIR. It includes 12 questions for quality evaluation and 4 questions for diversity assessment. We include examples for quality and diversity evaluation of our questionnaire in Fig. 21. Finally, we report the percentage of the user preference from 220 responses for each method and for both quality and diversity metrics in Tab. 2 in the main paper.

L. Related Work

Zero-shot Generative Model Adaptation Zero-shot generative model adaptation is the task of adapting the source domain knowledge of a well-trained generator to the target domain without accessing any target samples. Unlike the zero-shot image editing methods [45] [50] where available modifications are constrained in the domain of the pre-trained generator, zero-shot generator adaptation can perform out-of-domain manipulation by directly optimizing

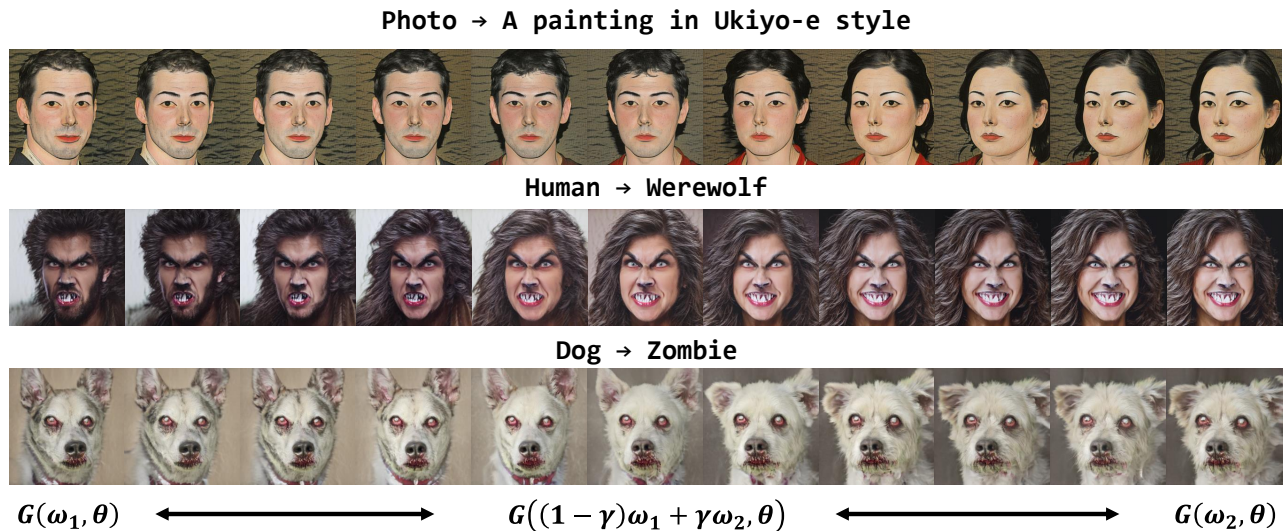


Figure 16. Latent space interpolation. For each row, the left-most column and right-most column are respectively two images synthesized with two different latent codes. The remaining columns refer to images synthesized with interpolated latent codes.

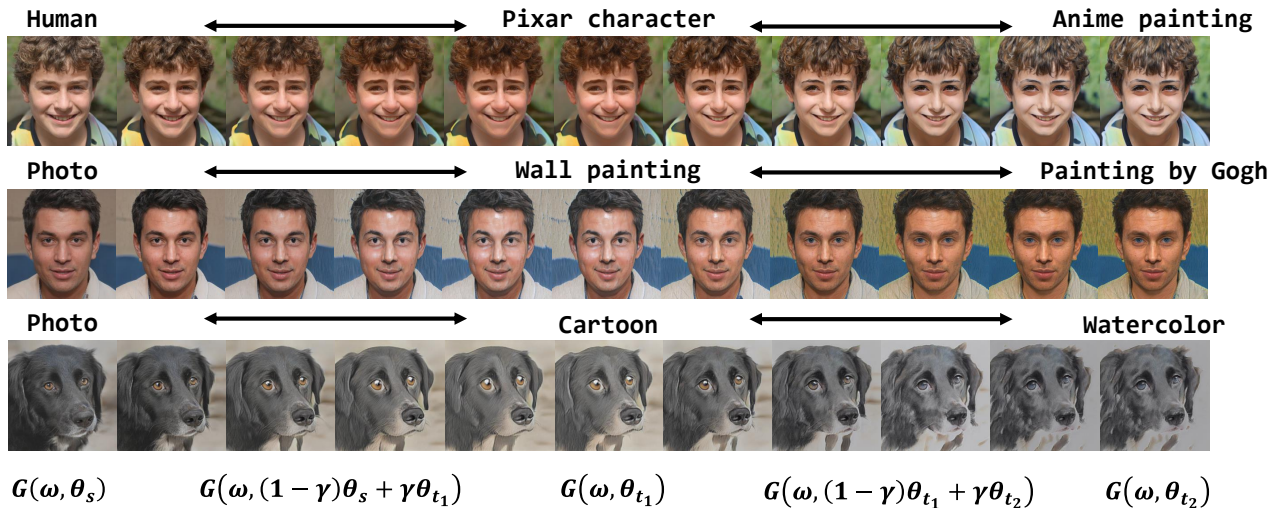


Figure 17. Cross-model interpolation. In each row, the left-most image is generated by the source generator. The middle and the right-most images are synthesized by two different target domain generators. The other images represent cross-model interpolations between two different domains.

the generator parameters. Previous works [15, 19, 21] utilized the cross-modal representation in CLIP [47] to bypass the need for extensive data collection. Specifically, NADA [15] first proposes to use the embedding offset of textual description in the CLIP space to describe the difference between source and target domains. By assuming the text offset and image offset are well-aligned in CLIP space, it uses the text offset as adaptation direction and op-

timizes the trainable generator to align image offset with text offset. IPL [19] points out that adaptation directions in NADA for diverse image samples is computed from one pair of manually designed prompts, which will cause mode collapse, therefore they produce different adaptation directions for each sample. Similarly, SVL [21] use embedding statistics (mean and variance) for producing adaptation direction instead of only mean of embeddings in NADA to

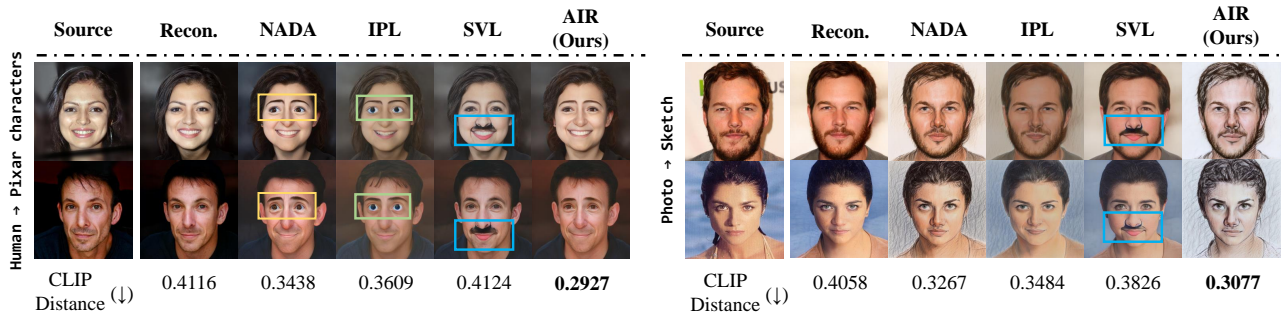


Figure 18. Image manipulation with GAN. The reference image are the same as in Fig. 1, 5.

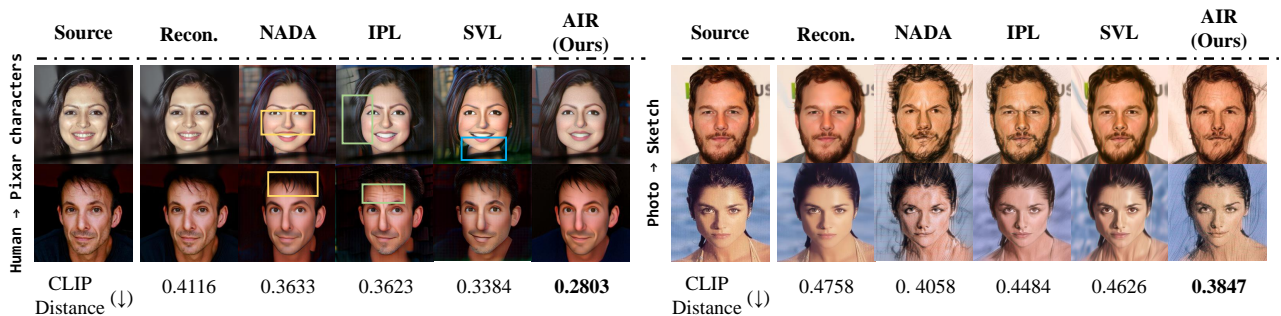


Figure 19. Diffusion model image manipulation. The reference images are the same as in Fig. 1, 5.

prevent mode collapse.

However, the adaptation direction in previous work only focuses on the source and target domains and computes once before the generator adaptation. More importantly, all these methods assume the image and text offsets in the CLIP space are well aligned. In this paper, we draw inspiration from a similar problem called analogical reasoning in NLP, and empirically discover that the alignment of image and text offset in CLIP space is correlated to the concept proximity in CLIP space. Based on this finding, we proposed a method that iteratively updates the adaptation direction, which is more aligned with the image offset and more accurate for zero-shot adaptation with directional loss.

Analogical Reasoning Research in NLP has shown that word representations of language models are surprisingly good at capturing semantic regularities in language [7, 53]. Specifically, analogical reasoning [33, 39–41], utilizing the semantic regularities of word representations, aims to solve analogy tasks by using one pair of word vectors to identify the unknown member of a different pair of words, commonly via alignment of offsets. This is commonly modeled as using the vector offset between two words $a' - a$, and applying it to a new word b to predict the missing word b' that pair with b , as illustrated by the famous example of

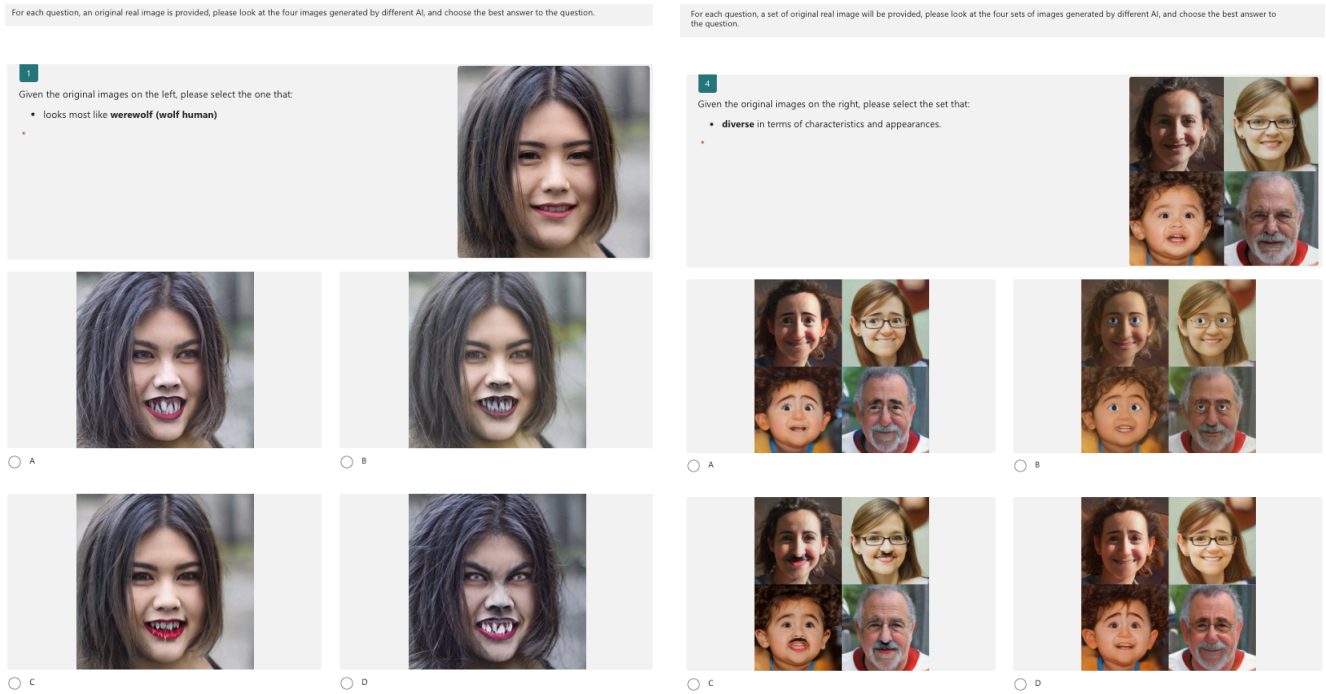
using $v(\text{"Man"}) - v(\text{"Woman"})$ and $v(\text{"King"})$ to identify $v(\text{"Queen"})$, where $v(\cdot)$ denotes word representation. This approach attracted a lot of attention for the vital role that analogical reasoning plays in human cognition for discovering new knowledge and understanding new concepts. It is already used in many downstream NLP tasks, such as splitting compounds [8], semantic search [6], cross-language relational search [12], etc.

Importantly, previous works [28, 34, 54] demonstrate that the effectiveness of analogical reasoning varies across different categories and semantic relations. More recent studies [14, 48], present a series of experiments performed with BATS dataset [17] on various pre-trained vector space, e.g., GloVe [46], Word2Vec [40], and Skip-gram [39], indicate that it is more effective to use $a' - a$ and b to determine b' when b and b' are close in vector space; and less so when b and b' are more apart.

Inspired by these studies, in this work, we perform an empirical study of offset misalignment in CLIP space and observe that for distant concepts in CLIP, image and text offset suffer from more misalignment, while closely related concepts suffer less. Based on our analysis, we proposed a method that iteratively refined the text offset for adaptation, which results in less offset misalignment and leads to



Figure 20. Additional results of image manipulation with diffusion model.



(a) Qualitative evaluation

(b) Diversity assessment

Figure 21. Examples of user study on (a) Quality assessment and (b) Diversity assessment.

a better generative model adaptation with directional loss.

M. Limitation

Our proposed iterative refinement method seeks to improve the quality of zero-shot adaptation. As noted by [19],

achieving adaptation across large domain gaps, such as Human to Cat, is particularly challenging. Similar to previous work, our approach necessitates that the trained generator somewhat closely approximates the target domain before initiating iterative refinement. Additionally, while our experiments on 26 different setups are comprehensive com-

Models	License
StyleGAN2 [24]	Nvidia Source Code License
CLIP [47]	MIT License
StyleGAN2-pytorch [24]	MIT License
e4e [52]	MIT License
StyleGAN-NADA [15]	MIT License
IPL [19]	MIT License
Datasets	License
FFHQ [5]	CC BY-NC-SA 4.0
AFHQ [1]	CC BY NC 4.0

Table 13. Sources and licenses of the utilized models and datasets

pared to previous work, more setups can be experimented to understand the limitations.

N. Social Impact

The AIR methodology holds potential for enhancing artistic image synthesis in social media contexts and could serve as a beneficial data augmentation tool in other computer vision tasks such as recognition and detection. However, its capability to generate realistic images from real-world data raises ethical considerations. It is crucial to address these issues thoughtfully to prevent misuse and ensure responsible application of this technology.

O. Licenses

In Table 13, we specify the source and licenses of the models and datasets used in our work. Note that the FFHQ dataset consists of facial images collected from Flickr, which are under permissive licenses for non-commercial purposes.